LETTER

doi:10.1038/nature16460

Interleukin-22 promotes intestinal-stem-cell-mediated epithelial regeneration

Caroline A. Lindemans[1,2]*, Marco Calafiore[1]*, Anna M. Mertelsmann[1]*, Margaret H. O'Connor[1]*, Jarrod A. Dudakov[3,4], Robert R. Jenq[1,5], Enrico Velardi[3], Lauren F. Young[3], Odette M. Smith[3], Gillian Lawrence[1], Juliet A. Ivanov[1], Ya-Yuan Fu[1], Shuichiro Takashima[1], Guoqiang Hua[6,7], Maria L. Martin[7], Kevin P. O'Rourke[8], Yuan-Hung Lo[9], Michal Mokry[2], Monica Romera-Hernandez[10], Tom Cupedo[10], Lukas E. Dow[5], Edward E. Nieuwenhuis[2], Noah F. Shroyer[9], Chen Liu[11], Richard Kolesnick[7], Marcel R. M. van den Brink[1,3]§ & Alan M. Hanash[1]§

Epithelial regeneration is critical for barrier maintenance and organ function after intestinal injury. The intestinal stem cell (ISC) niche provides Wnt, Notch and epidermal growth factor (EGF) signals supporting Lgr5$^+$ crypt base columnar ISCs for normal epithelial maintenance[1,2]. However, little is known about the regulation of the ISC compartment after tissue damage. Using *ex vivo* organoid cultures, here we show that innate lymphoid cells (ILCs), potent producers of interleukin-22 (IL-22) after intestinal injury[3,4], increase the growth of mouse small intestine organoids in an IL-22-dependent fashion. Recombinant IL-22 directly targeted ISCs, augmenting the growth of both mouse and human intestinal organoids, increasing proliferation and promoting ISC expansion. IL-22 induced STAT3 phosphorylation in Lgr5$^+$ ISCs, and STAT3 was crucial for both organoid formation and IL-22-mediated regeneration. Treatment with IL-22 *in vivo* after mouse allogeneic bone marrow transplantation enhanced the recovery of ISCs, increased epithelial regeneration and reduced intestinal pathology and mortality from graft-versus-host disease. ATOH1-deficient organoid culture demonstrated that IL-22 induced epithelial regeneration independently of the Paneth cell niche. Our findings reveal a fundamental mechanism by which the immune system is able to support the intestinal epithelium, activating ISCs to promote regeneration.

The epithelial layer in the gastrointestinal tract represents a fundamental line of defence against potential enteric pathogens. Paneth cells contribute to this defence by producing antimicrobial molecules and by providing an epithelial niche for Lgr5$^+$ ISCs that maintain the epithelium[2]. ISCs are critical for damage-induced intestinal regeneration[5], but the mechanisms regulating ISC function and inducing epithelial regeneration after tissue damage remain poorly understood. Furthermore, although epithelial barrier function is a core component of intestinal immunity, little is known about the role of the immune system in regulating the ISC compartment. Group 3 ILCs (ILC3s) are crucial for maintaining gastrointestinal epithelial integrity and barrier function in several experimental models of intestinal injury[3]. Tissue-resident ILC3s are potent producers of IL-22 after damage, and IL-22 expression is associated with reduced injury in colitis as well as several non-intestinal tissue damage models[3,4,6–9]. However, although the IL-22 receptor (IL-22R) is present in many epithelial tissues, the specific cellular targets and mechanisms of IL-22 inducing tissue recovery are largely unknown. Using an organoid model of *ex vivo* epithelial regeneration[10], we examined whether ILCs and IL-22 could regulate the ISC compartment.

We first sorted mouse small intestine (SI) lamina propria lymphocytes (LPLs), which include both innate and adaptive lymphoid cells capable of producing IL-22 (ref. 4), and cultured them with freshly isolated mouse SI crypts in standard organoid media containing EGF, Noggin and R-spondin-1 (ENR). An IL-23-based cytokine cocktail was included for IL-22 induction. Two-dimensional perimeter tracing (Extended Data Fig. 1a) indicated that co-culture with wild-type LPLs significantly increased organoid size (Fig. 1a). By contrast, LPLs isolated from IL-22-deficient (*Il22*$^{-/-}$) mice failed to augment organoid size (Fig. 1a). To evaluate the role of ILC3s in organoid growth, SI lamina propria CD45$^+$CD3$^-$RORγt$^+$ ILC3s were isolated from Rorc(γt)-GFP (green fluorescent protein) reporter mice and cultured with SI crypts. ILC3s significantly increased SI organoid size, and this was inhibited by an anti-IL-22 neutralizing antibody (Fig. 1b).

Given that IL-22 was essential for ILC-mediated augmentation of organoid size, we focused on studies with recombinant mouse (rm)IL-22. SI crypts cultured with rmIL-22 yielded substantially larger organoids in a concentration-dependent fashion (Fig. 1c, d and Extended Data Fig. 1b). While high concentrations of IL-22 reduced the efficiency of organoid generation from SI crypts, culture with 1–5 ng ml^{-1} rmIL-22 increased organoid size without affecting organoid formation (Extended Data Fig. 1c). IL-22 also increased large intestine organoid size without affecting efficiency (Fig. 1e and Extended Data Fig. 1d), and culture with IL-22 augmented crypt budding in both small and large intestine organoids (Fig. 1f). Furthermore, recombinant human (rh)IL-22 significantly increased the size of human intestinal organoids generated from primary duodenal tissue (Fig. 1g and Extended Data Fig. 1e).

Wnt/β-catenin signalling is essential for ISC maintenance and organoid function *ex vivo*[10]. However, we found no evidence of enhanced production of molecules in the Wnt/β-catenin pathway within SI organoids cultured with IL-22, including no difference in expression of WNT3, β-catenin or the downstream target AXIN2 (Extended Data Fig. 1f). Consistent with this, IL-22 could not replace R-spondin-1, an agonist of Wnt/β-catenin signalling, as its removal eliminated SI organoid growth even in the presence of IL-22 (Extended Data Fig. 1g). Additionally, we found no IL-22-induced activation of gene expression in the Notch pathway, which is also critical for ISC maintenance, or activation of gene expression

[1]Department of Medicine, Memorial Sloan Kettering Cancer Center, New York, New York 10065, USA. [2]Department of Pediatrics, University Medical Center Utrecht, 3508 AB Utrecht, The Netherlands. [3]Department of Immunology, Memorial Sloan Kettering Cancer Center, New York, New York 10065, USA. [4]Department of Anatomy and Developmental Biology, Monash University, Clayton 3800, Australia. [5]Department of Medicine, Weill Cornell Medicine, New York, New York 10021, USA. [6]Department of Radiation Oncology, Memorial Sloan Kettering Cancer Center, New York, New York 10065, USA. [7]Department of Molecular Pharmacology, Memorial Sloan Kettering Cancer Center, New York, New York 10065, USA. [8]Department of Cancer Biology & Genetics, Memorial Sloan Kettering Cancer Center, New York, New York 10065, USA. [9]Department of Medicine, Baylor College of Medicine, Houston, Texas 77030, USA. [10]Department of Hematology, Erasmus University Medical Center, 3000 CA Rotterdam, The Netherlands. [11]Department of Pathology, Immunology and Laboratory Medicine, University of Florida College of Medicine, Gainesville, Florida 32610, USA.
*These authors contributed equally to this work.
§These authors jointly supervised this work.

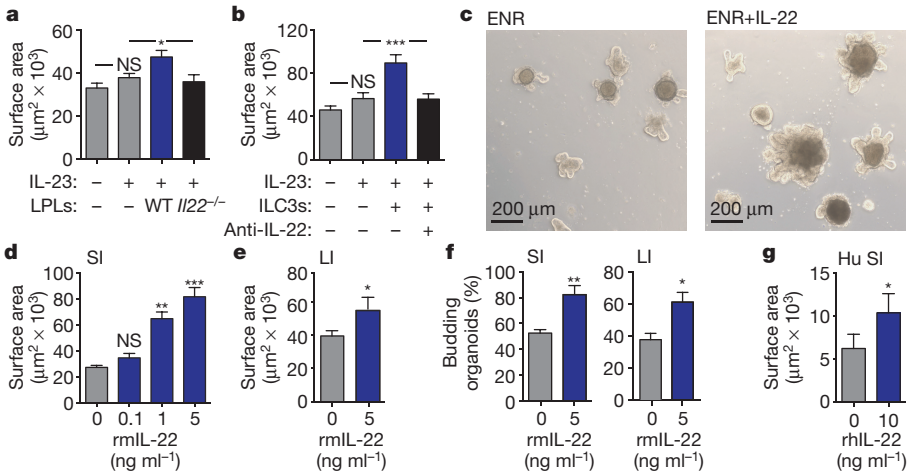

Figure 1 | IL-22 increases growth of intestinal organoids. a, Size of SI organoids cultured in ENR with IL-23-containing cytokine cocktail with/without LPLs; $n = 62$ (control), $n = 72$ (IL-23), $n = 29$ (wild-type (WT) LPLs), $n = 34$ ($Il22^{-/-}$ LPLs) organoids per group; one of two experiments. **b**, Size of SI organoids cultured with/without ILC3s and anti-IL-22 neutralizing antibody; $n = 47$ (control), $n = 55$ (IL-23), $n = 43$ (ILC3s), $n = 38$ (anti-IL-22) organoids per group; one of two experiments. **c**, SI organoids cultured with/without rmIL-22 (5 ng ml^{-1}) for 7 days. **d**, **e**, Size of organoids cultured with/without rmIL-22 for 7 days; $n = 114$ (control), $n = 50$ (0.1 ng ml^{-1}), $n = 47$ (1 ng ml^{-1}), $n = 44$ (5 ng ml^{-1}) SI organoids per group (**d**); $n = 115$ (control), $n = 61$ (IL-22) large intestine (LI) organoids per group (**e**). **f**, New crypt formation (budding) of small (day 4) and large (day 7) intestine organoids; $n = 6$ mice per group. **g**, Size of human (Hu) SI organoids cultured with/without rhIL-22 (10 ng ml^{-1}) in standard expansion medium; $n = 38$ (control), $n = 67$ (IL-22) organoids per group. Data are mean and s.e.m.; comparisons performed with *t*-tests (two groups) or analysis of variance (ANOVA) (multiple groups). NS, not significant; $*P < 0.05$, $**P < 0.01$, $***P < 0.001$. Data combined from at least three independent experiments unless otherwise stated.

for SLIT2 or ROBO1, although they can regulate ISC recovery from damage induced by chemotherapy and radiation[11] (Extended Data Fig. 1h). Consistently, there was also no increase in Wnt or Notch pathway gene expression in large intestine organoids (Extended Data Fig. 1i). However, culture with IL-22 increased SI organoid mRNA levels of the innate antimicrobial molecules *Reg3b* and *Reg3g* (Extended Data Fig. 1j), the expression of which is dependent on STAT3 signalling[12].

Little is known about JAK/STAT signalling within ISCs, although it has been reported that STAT3 may be important for ISC maintenance[13]. We evaluated STAT3 signalling in SI organoids and found that IL-22 increased the phosphorylation of STAT3 Tyr705 (Extended Data Fig. 2a). Furthermore, treatment with the STAT3 inhibitor Stattic significantly impaired SI organoid growth (Fig. 2a and Extended Data Fig. 2b). However, IL-22 can also promote epithelial STAT1 signalling[14], which Stattic has inhibitory activity against[15]. Indeed, organoid STAT3 and STAT1 were both phosphorylated in response to IL-22, and inhibited by Stattic (Fig. 2b). To determine their relative importance for IL-22-induced epithelial regeneration, we assessed the growth of organoids with genetic deletion of either *Stat1* or *Stat3*. Despite the induction of phosphorylated (p) STAT1 by IL-22, SI crypts from $Stat1^{-/-}$ mice demonstrated intact organoid growth and response to IL-22 (Fig. 2c and Extended Data Fig. 2c). As $Stat3^{-/-}$ mice are not viable, we next cultured SI crypt cells from $Stat3^{fl/fl}$ mice with adenoviral-Cre (adeno-Cre) to delete STAT3. Crypt cells from wild-type mice demonstrated intact organoid growth and IL-22 response despite *in vitro* infection with adeno-Cre (Fig. 2d). Additionally, uninfected $Stat3^{fl/fl}$ crypt cells demonstrated normal organoid growth and response to IL-22 (Extended Data Fig. 2d, e). However, crypt cells from $Stat3^{fl/fl}$ mice failed to generate organoids after infection with adeno-Cre, and IL-22 failed to recover organoid growth or augment organoid size (Fig. 2d).

$Lgr5^+$ ISCs can generate all cell types of mature intestinal epithelium *ex vivo* and *in vivo*[1,10]. To evaluate whether STAT3 was important for ISCs during tissue damage *in vivo*, we performed a gene set enrichment analysis (GSEA), assessing expression of a published $Lgr5^+$ ISC gene signature (Gene Expression Omnibus (GEO) data set GSE33948)[16] in another data set of wild-type ($Stat3^{fl/fl}$) versus epithelial STAT3-deficient ($Stat3^{fl/fl}$;*Villin-Cre*) mice with dextran sulfate sodium (DSS) colitis (GSE15955)[12]. Expression of the $Lgr5^+$ ISC gene signature was significantly reduced in STAT3-deficient mice with colitis (Fig. 2e). This was validated with a second independently established $Lgr5^+$ ISC gene signature (GEO data set GSE23672)[16], while no significant changes were seen with a negative-control Paneth cell gene signature (GEO data set GSE39915)[17] (Extended Data Fig. 2f, g). Given the induction of pSTAT3 by IL-22 and the importance of STAT3 for ISC gene signature maintenance, we examined the effect of IL-22 during regeneration using purified ISCs. We isolated Lgr5–GFP SI ISCs by fluorescence-activated cell sorting (FACS) and cultured purified ISCs under standard conditions[10] with or without IL-22. IL-22 significantly increased the budding of early organoids after just 4 days (Fig. 2f). Furthermore, as with crypt-derived organoids, 1 ng ml^{-1} rmIL-22 augmented the size of organoids generated from purified ISCs without affecting the efficiency of organoid formation (Fig. 2g and Extended Data Fig. 3a, b).

Consistent with increased size, IL-22 enhanced 5-ethynyl-2′-deoxyuridine (EdU) incorporation in SI organoids, demonstrating increased proliferation (Extended Data Fig. 4a, b). Hoechst staining revealed an IL-22-dependent increase in G2/M populations after 2 days in culture (Fig. 2h), and IL-22 treatment rapidly reduced expression of key cell cycle checkpoint molecules *Cdkn1a* and *Cdkn2d* in both small and large intestine organoids (Extended Data Fig. 4c, d). Furthermore, IL-22 expanded Lgr5–GFP^{high} ISCs in SI organoids (Fig. 2i) and increased expansion of SI organoids over several passages in culture (Fig. 2j). Next, we evaluated the ISC compartment after radiation injury. Pre-treatment with rmIL-22 increased the percentage of dissociated SI crypt cells that were viable in culture after *ex vivo* irradiation, as measured by MTT reduction (Extended Data Fig. 5a). Consistent with this, IL-22 treatment increased the number of organoids that could grow from single cells 2 days after irradiation (Extended Data Fig. 5b). This was more evident with increasing doses of irradiation, and protection was present even 7 days after irradiation (Extended Data Fig. 5c). Accordingly, irradiation was found to increase the expression of *Il22ra1* within intestinal crypts (Extended Data Fig. 5d).

We next evaluated the effect of IL-22 *in vivo* after tissue damage using a clinically relevant mouse graft-versus-host disease (GVHD) model. T-cell-depleted (TCD) marrow from LP mice was transplanted with or without purified LP T cells into lethally irradiated C57BL/6 (B6) recipients (H-2^b into H-2^b). Mice receiving allogeneic T cells for

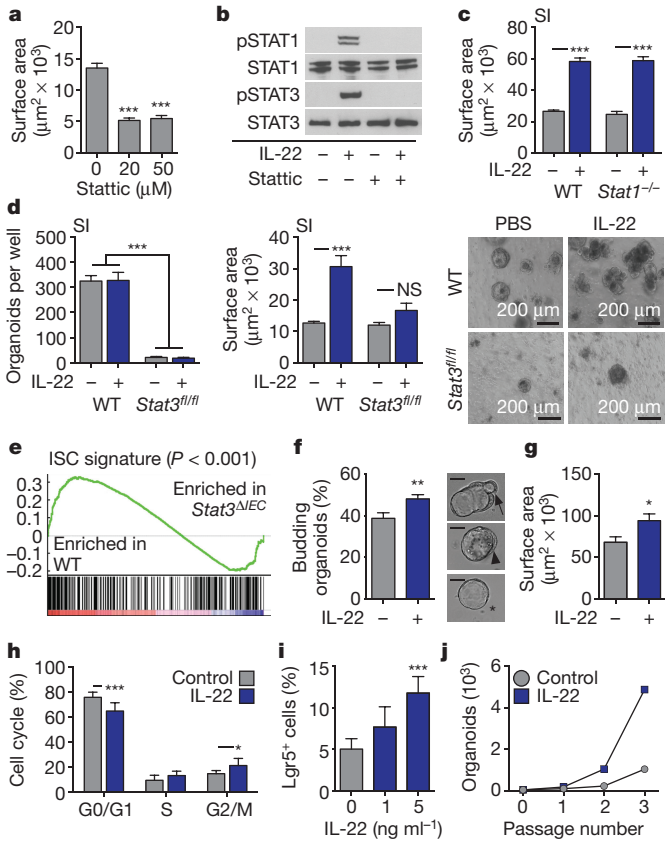

Figure 2 | IL-22 activates organoid STAT3 signalling and augments ISC regeneration. a, SI organoid size, after 4 days with/without Stattic; $n = 174$ (control), $n = 134$ (20 μM), $n = 102$ (50 μM) organoids per group. **b**, Crypt pSTAT western blots after 30 min incubation with rmIL-22 (5 ng ml^{-1}) with/without Stattic; one of three experiments. **c**, Size of day 7 wild-type and *Stat1*$^{-/-}$ SI organoids with/without rmIL-22 (5 ng ml^{-1}); $n = 821$ (wild type), $n = 503$ (wild type plus IL-22), $n = 432$ (*Stat1*$^{-/-}$), $n = 269$ (*Stat1*$^{-/-}$ plus IL-22) organoids per group. **d**, Day 5 *Stat3*$^{fl/fl}$ SI organoids cultured with adeno-Cre with/without rmIL-22 (5 ng ml^{-1}); numbers per well, $n = 6$ wells per group; size, $n = 253$ (wild type), $n = 49$ (wild type plus IL-22), $n = 38$ (*Stat3*$^{fl/fl}$), $n = 38$ (*Stat3*$^{fl/fl}$ plus IL-22) organoids per group; images (right) representative of three experiments. **e**, GSEA of ISC signature genes in wild-type versus *Stat3*$^{fl/fl}$;*Villin-Cre* (*Stat3*$^{\Delta IEC}$) mice with DSS colitis; one analysis, nominal *P* value shown. **f**, **g**, Organoids from sorted SI Lgr5–GFP^{+} ISCs cultured with/without rmIL-22 (1 ng ml^{-1}). **f**, Organoid budding, percentage of total organoids per well (day 4, $n = 11$ wells per group). Representative images (right) of early budding indicate: early organoid without budding (asterisk); polarization before budding (arrowhead); budding at site of polarization (arrow). Scale bars, 50 μm. **g**, Organoid area (day 13), $n = 54$ organoids per group. **h**, Cell cycle FACS of SI organoid cells cultured with/without rmIL-22 (5 ng ml^{-1}); $n = 7$ mice per group. **i**, FACS analysis of Lgr5–GFP^{high} ISCs in organoids cultured with/without rmIL-22; $n = 6$ mice per group. **j**, Organoid expansion with serial passaging with/without rmIL-22 (1 ng ml^{-1}); one of two experiments. Data are mean and s.e.m.; comparisons performed with *t*-tests (two groups) or ANOVA (multiple groups); $^{*}P < 0.05$, $^{**}P < 0.01$, $^{***}P < 0.001$. Data combined from at least two independent experiments unless otherwise stated. For western blot source data, see Supplementary Fig. 1.

GVHD induction were treated with 4 μg rmIL-22 or PBS daily via intraperitoneal (i.p.) injection starting 7 days after bone marrow transplantation (BMT). Treatment with IL-22 reduced histopathological evidence of GVHD in the small and large intestine (Fig. 3a), including a reduction in apoptosis within crypt epithelium (Extended Data Fig. 6a, b). GVHD pathology was reduced despite an intact alloimmune response, as evidenced by similar T cell subset distribution, activation markers and gut homing molecules, as well as similar systemic and gastrointestinal expression of inflammatory cytokines (Extended Data Fig. 6c, d). However, IL-22 treatment did increase SI expression of *Reg3b* and *Reg3g* mRNA (Fig. 3b). Consistent with previous findings[18], we found that REG3β was primarily expressed by enterocytes in allogeneic BMT recipients, including after treatment with IL-22 (Extended Data Fig. 6e).

GVHD is associated with a loss of both ISCs[19,20] and niche-forming Paneth cells[21,22], and T-cell-replete BMT led to a significant loss of Lgr5-LacZ^{+} SI ISCs 3 weeks after transplantation (Fig. 3c). However, IL-22 treatment increased the recovery of Lgr5^{+} ISCs (Fig. 3c). This was associated with increased regeneration as evidenced by increased crypt height, including the transit-amplifying compartment (Fig. 3d). Paneth cells support Lgr5^{+} ISCs through the delivery of Wnt, Notch ligand and EGF signals[2]. Additionally, IL-22 is thought to regulate Paneth cell production of innate antimicrobial molecules. We thus proposed that IL-22 could support ISC recovery after BMT by improving the function of the stem-cell niche. Consistent with previous clinical and experimental studies[21–23], minor antigen-mismatched BMT led to a reduction in Paneth cells 3 weeks after transplantation (Fig. 3e). However, IL-22 administration did not increase recovery of Paneth cells (Fig. 3e), mRNA expression of *Wnt3* or *Egf* (Extended Data Fig. 6f, g), or expression of Notch ligand target *Hes1* (Extended Data Fig. 6h). Furthermore, although stroma can support ISC Wnt signalling *in vivo* independently of Paneth cells[24], we found no change in expression of stromal R-spondin-3 after IL-22 treatment post-BMT, and no change in expression of Wnt pathway genes regardless of the upstream source (Extended Data Fig. 6i–k).

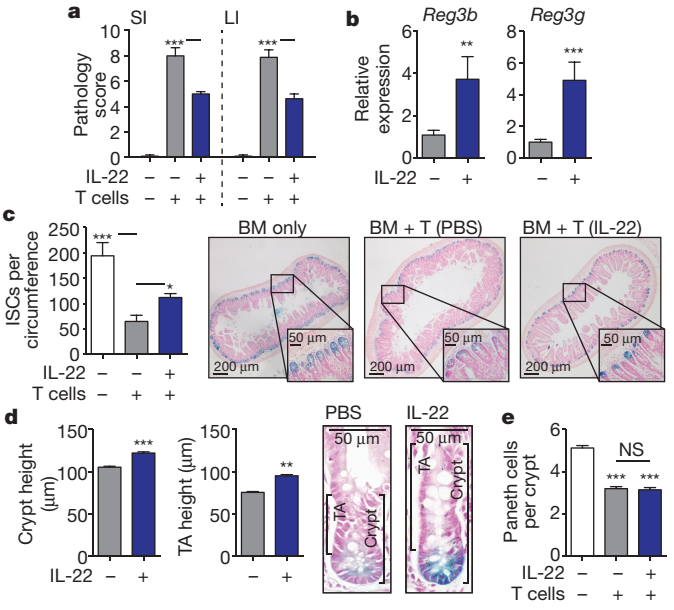

Figure 3 | IL-22 reduces intestinal pathology and increases ISC recovery after *in vivo* tissue damage. LP into B6 BMT; recipients treated daily with PBS or 4 μg rmIL-22 i.p. starting 7 days after BMT. **a**, Intestinal GVHD histopathology score, 3 weeks after BMT; $n = 10$ (TCD bone marrow (BM) only), $n = 9$ (BM plus T (PBS)), $n = 8$ (BM plus T (IL-22)) mice per group; Kruskal–Wallis analysis. **b**, qPCR of *Reg3b* and *Reg3g* in SI tissue 3 weeks after BMT; $n = 9$ (PBS) and $n = 10$ (IL-22) mice per group; Mann–Whitney *U* analysis. **c**, **d**, B6 Lgr5-LacZ recipients. **c**, SI ISC frequency 3 weeks after BMT; Kruskal–Wallis analysis of $n = 8$ (TCD BM only), $n = 20$ (BM plus T (PBS)), or $n = 20$ (BM plus T (IL-22)) independent sections (four sections per recipient from 2–5 mice per group); one of two experiments. **d**, Crypt and transit-amplifying (TA) heights 3 weeks after BMT, representative images on right; *t*-test analyses of $n = 285$ (PBS) versus $n = 324$ (IL-22) crypts, and $n = 168$ (PBS) versus $n = 224$ (IL-22) transit-amplifying compartments (one section per mouse, >10 mice per group). **e**, SI lysozyme^{+} Paneth cell frequency; Kruskal–Wallis analysis of $n = 73$ (TCD BM only), $n = 89$ (BM plus T (PBS)), and $n = 88$ (BM plus T (IL-22)) crypts (5–8 mice per group). Data are mean and s.e.m.; $^{*}P < 0.05$, $^{**}P < 0.01$, $^{***}P < 0.001$. Data combined from at least two independent experiments unless otherwise stated.

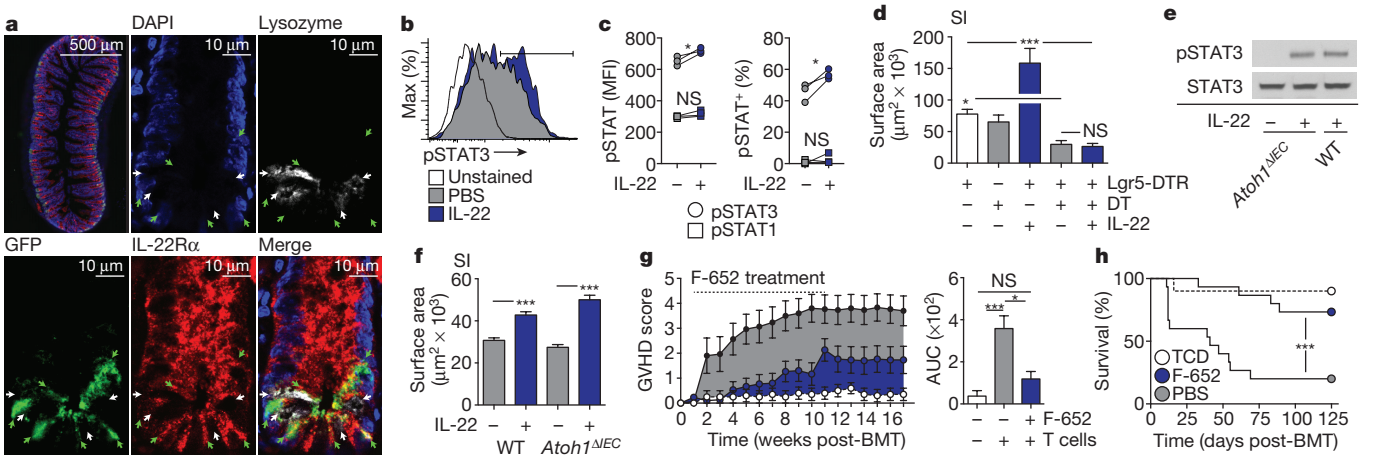

Figure 4 | IL-22 directly promotes ISC-dependent epithelial regeneration. a, Immunofluorescent staining of IL-22Rα1, GFP and lysozyme in SI sections from Lgr5–GFP mice; green arrows, Lgr5–GFP$^+$ ISCs; white arrows; lysozyme$^+$ Paneth cells. DAPI, 4′,6-diamidino-2-phenylindole. **b**, **c**, Phosflow analysis of Lgr5–GFP$^+$ SI crypt cells after 30 min with/without rmIL-22 (20 ng ml^{-1}). **b**, pSTAT3 histogram; representative of four experiments. **c**, pSTAT median fluorescence intensity (MFI) and percentage pSTAT$^+$; $n = 3$ mice per group; representative of two experiments. **d**, Size of wild-type and Lgr5-DTR day 5 SI organoids cultured with diphtheria toxin (DT; 1 ng μl^{-1}) to deplete Lgr5$^+$ cells with/without rmIL-22 (5 ng ml^{-1}); one of three experiments; $n = 65$ (wild type), $n = 25$ (wild type plus DT), $n = 28$ (DTR plus IL-22), $n = 18$ (DTR plus diphtheria toxin), $n = 40$ (DTR, diphtheria toxin and IL-22) organoids per group. **e**, **f**, Paneth-cell-deficient *Atoh1*$^{\Delta IEC}$ SI organoids cultured in WNT3-supplemented ENR with/without rmIL-22 (5 ng ml^{-1}). **e**, STAT3 western blots after 30 min culture with rmIL-22; one of four experiments. **f**, Day 7 organoid size; $n = 466$ (wild type), $n = 531$ (wild type plus IL-22), $n = 197$ (*Atoh1*$^{\Delta IEC}$), $n = 491$ (*Atoh1*$^{\Delta IEC}$ plus IL-22) organoids per group. **g**, **h**, LP into B6 BMT, with/without F-652 (100 μg kg^{-1} subcutaneous, every other day starting day 7 after BMT, 10-week course); $n = 10$ (TCD BM only), $n = 15$ (BM plus T (PBS)), $n = 15$ (BM plus T (IL-22)). **g**, Clinical signs of GVHD and area under the curve (AUC) analysis of GVHD scoring. **h**, Percentage survival. Data are mean and s.e.m.; comparisons performed with *t*-tests (two groups), ANOVA (multiple groups), or log–rank analysis (**h**); $^*P < 0.05$, $^{***}P < 0.001$. Data combined from at least two independent experiments unless otherwise stated. For western blot source data, see Supplementary Fig. 1.

Given that IL-22 treatment appeared to improve ISC numbers without improving niche function in BMT recipients, we sought to evaluate how IL-22 was targeting the ISC compartment. Consistent with the *in vivo* findings, IL-22 had no effect on Paneth cell frequency or α-defensin-1 expression within SI organoids cultured *ex vivo* (Extended Data Fig. 7a, b). Immunofluorescent staining for IL-22Rα1 and the Paneth cell marker lysozyme using SI sections from Lgr5–GFP reporter mice indicated substantial IL-22R staining within crypts and enterocytes at the villous base, but not on lysozyme$^+$ Paneth cells (Fig. 4a). Using flow cytometry, there was also little evidence for expression of IL22Rα1 on Paneth cells at baseline or after radiation injury and no evidence of pSTAT3 in Paneth cells in response to IL-22 (Extended Data Fig. 7c–e). By contrast, IL22Rα1 was identified in the transit-amplifying progenitor compartment and on Lgr5–GFP$^+$ ISCs (Fig. 4a). IL-22R expression in Lgr5$^+$ cells was confirmed by quantitative PCR (qPCR) after sorting for Lgr5–GFP$^+$ cells (Extended Data Fig. 8a, b). Furthermore, SI crypt cells from Lgr5–GFP reporter mice demonstrated increased STAT3 Tyr705 phosphorylation within GFP$^+$ cells after incubation with IL-22, indicating functional IL-22R signalling in ISCs (Fig. 4b, c). STAT3 phosphorylation was a specific response, as there was no effect of IL-22 on pSTAT1 in Lgr5$^+$ cells (Fig. 4c).

IL-22R expression and STAT3 phosphorylation suggested that IL-22 might promote regeneration via direct targeting of ISCs. To investigate the role of ISCs and Paneth cells in IL-22-mediated regeneration further, we assessed organoid growth when either cell population was depleted. Treatment of transgenic mice expressing the diphtheria toxin receptor (Lgr5-DTR) with diphtheria toxin leads to a rapid deletion of Lgr5$^+$ cells[25]. Deletion of Lgr5$^+$ cells *ex vivo* by culturing Lgr5-DTR SI organoids with diphtheria toxin impaired epithelial regeneration as evidenced by a reduction in organoid size and efficiency (Fig. 4d and Extended Data Fig. 9a). Although IL-22 increased the size of Lgr5-DTR organoids cultured without diphtheria toxin, IL-22 failed to increase the size or maintain the numbers of Lgr5-DTR organoids cultured with diphtheria toxin (Fig. 4d and Extended Data Fig. 9a), indicating that Lgr5$^+$ cells are essential for IL-22-mediated epithelial regeneration.

We next investigated the functional importance of Paneth cells for IL-22-mediated regeneration by culturing organoids with IL-22 after inducible Paneth cell depletion. Paneth cells were deleted *in vivo* after tamoxifen treatment of *Atoh1*$^{fl/fl}$;*Villin-Cre*^{ERT2} (*Atoh1*$^{\Delta IEC}$) mice[26]. IL-22 led to robust STAT3 phosphorylation within *Atoh1*$^{\Delta IEC}$ SI organoids, confirming that Paneth cells were not essential for IL-22-mediated intracellular signalling, and *Atoh1*$^{\Delta IEC}$ organoids demonstrated an intact growth response to IL-22 (Fig. 4e, f and Extended Data Fig. 9b). Additionally, we found that IL-22 could augment the size of organoids cultured without EGF (Extended Data Fig. 9c, d). These findings indicated that the Paneth cell niche was not required for IL-22-mediated epithelial regeneration, and IL-22 could promote the growth of organoids cultured without addition of the niche-derived growth factor EGF.

Recent reports have suggested that T-cell-derived IL-22 may contribute to GVHD, as might peri-transplant administration of IL-22 to MHC-mismatched BMT recipients[27,28]. However, IL-22-producing ILCs are eliminated in GVHD[19], ILC deficiency is associated with increased clinical GVHD[29], and gastrointestinal damage may be central to the pathogenesis of systemic GVHD[30]. We thus proposed that stimulating regeneration with IL-22 after the initiation of GVHD-related tissue damage may be therapeutically beneficial. Given the improved pharmacological stability of Fc-fusion molecules, we evaluated the potential of F-652, a rhIL-22-dimer and Fc-fusion protein, for treatment of systemic GVHD. First, we found that F-652 had activity in mouse epithelial regeneration, augmenting the growth of both small and large intestine organoids without evidence of toxicity (Extended Data Fig. 10a–d). Second, treatment of Lgr5-LacZ reporter mice with F-652 significantly protected SI Lgr5$^+$ crypt cells from radiation injury *in vivo* (Extended Data Fig. 10e, f). We next investigated an early intervention model for GVHD, treating allogeneic BMT recipients (LP into B6) with F-652 starting 1 week after transplantation. Mice treated with F-652 demonstrated reduced systemic signs of GVHD and GVHD-related mortality compared to PBS-treated controls (Fig. 4g, h).

In summary, we found that IL-22 links immunity to epithelial regeneration by acting directly on ISCs. Purified ILCs enhanced organoid

growth in an IL-22-dependent fashion, and IL-22 augmented ISC-mediated epithelial regeneration, promoting cell cycle progression, epithelial proliferation and regeneration of the ISC pool. IL-22 induced STAT3 phosphorylation in Lgr5^{+} ISCs, and while IL-22 may not be its sole regulator in ISCs, STAT3 was essential for organoid growth and IL-22-dependent epithelial regeneration. Paneth cells, in contrast, were not required for IL-22-driven regeneration. Given the activation of IL-22 production and the upregulation of crypt IL-22R expression after tissue damage, these findings indicate that IL-22 contributes to damage-induced regulation of the ISC compartment. We conclude that in addition to the stromal and epithelial components of the ISC niche that are essential for normal epithelial maintenance, IL-22 provides evidence for an immunological contribution to the ISC niche that is activated to restore the epithelium after tissue injury. By acting directly on epithelial stem cells, the immune system is thus able to regulate intestinal regeneration and support the fundamental defence system provided by the integrity of the epithelial barrier.

Online Content Methods, along with any additional Extended Data display items and Source Data, are available in the online version of the paper; references unique to these sections appear only in the online paper.

Received 24 October 2014; accepted 18 November 2015.
Published online 9 December 2015.

1. Barker, N. *et al.* Identification of stem cells in small intestine and colon by marker gene *Lgr5*. *Nature* **449,** 1003–1007 (2007).
2. Sato, T. *et al.* Paneth cells constitute the niche for Lgr5 stem cells in intestinal crypts. *Nature* **469,** 415–418 (2011).
3. Sonnenberg, G. F. & Artis, D. Innate lymphoid cells in the initiation, regulation and resolution of inflammation. *Nature Med.* **21,** 698–708 (2015).
4. Dudakov, J. A., Hanash, A. M. & van den Brink, M. R. Interleukin-22: immunobiology and pathology. *Annu. Rev. Immunol.* **33,** 747–785 (2015).
5. Metcalfe, C., Kljavin, N. M., Ybarra, R. & de Sauvage, F. J. Lgr5^{+} stem cells are indispensable for radiation-induced intestinal regeneration. *Cell Stem Cell* **14,** 149–159 (2014).
6. Zheng, Y. *et al.* Interleukin-22 mediates early host defense against attaching and effacing bacterial pathogens. *Nature Med.* **14,** 282–289 (2008).
7. Zenewicz, L. A. *et al.* Interleukin-22 but not interleukin-17 provides protection to hepatocytes during acute liver inflammation. *Immunity* **27,** 647–659 (2007).
8. Aujla, S. J. *et al.* IL-22 mediates mucosal host defense against Gram-negative bacterial pneumonia. *Nature Med.* **14,** 275–281 (2008).
9. Dudakov, J. A. *et al.* Interleukin-22 drives endogenous thymic regeneration in mice. *Science* **336,** 91–95 (2012).
10. Sato, T. *et al.* Single Lgr5 stem cells build crypt-villus structures *in vitro* without a mesenchymal niche. *Nature* **459,** 262–265 (2009).
11. Zhou, W. J., Geng, Z. H., Spence, J. R. & Geng, J. G. Induction of intestinal stem cells by R-spondin 1 and Slit2 augments chemoradioprotection. *Nature* **501,** 107–111 (2013).
12. Pickert, G. *et al.* STAT3 links IL-22 signaling in intestinal epithelial cells to mucosal wound healing. *J. Exp. Med.* **206,** 1465–1472 (2009).
13. Matthews, J. R., Sansom, O. J. & Clarke, A. R. Absolute requirement for STAT3 function in small-intestine crypt stem cell survival. *Cell Death Differ.* **18,** 1934–1943 (2011).
14. Hernández, P. P. *et al.* Interferon-λ and interleukin 22 act synergistically for the induction of interferon-stimulated genes and control of rotavirus infection. *Nature Immunol.* **16,** 698–707 (2015).
15. Schust, J., Sperl, B., Hollis, A., Mayer, T. U. & Berg, T. Stattic: a small-molecule inhibitor of STAT3 activation and dimerization. *Chem. Biol.* **13,** 1235–1242 (2006).
16. Muñoz, J. *et al.* The Lgr5 intestinal stem cell signature: robust expression of proposed quiescent '+4' cell markers. *EMBO J.* **31,** 3079–3091 (2012).
17. van Es, J. H. *et al.* Dll1^{+} secretory progenitor cells revert to stem cells upon crypt damage. *Nature Cell Biol.* **14,** 1099–1104 (2012).
18. Eriguchi, Y. *et al.* Reciprocal expression of enteric antimicrobial proteins in intestinal graft-versus-host disease. *Biol. Blood Marrow Transplant.* **19,** 1525–1529 (2013).
19. Hanash, A. M. *et al.* Interleukin-22 protects intestinal stem cells from immune-mediated tissue damage and regulates sensitivity to graft versus host disease. *Immunity* **37,** 339–350 (2012).
20. Takashima, S. *et al.* The Wnt agonist R-spondin1 regulates systemic graft-versus-host disease by protecting intestinal stem cells. *J. Exp. Med.* **208,** 285–294 (2011).
21. Jenq, R. R. *et al.* Regulation of intestinal inflammation by microbiota following allogeneic bone marrow transplantation. *J. Exp. Med.* **209,** 903–911 (2012).
22. Eriguchi, Y. *et al.* Graft-versus-host disease disrupts intestinal microbial ecology by inhibiting Paneth cell production of α-defensins. *Blood* **120,** 223–231 (2012).
23. Levine, J. E. *et al.* Low Paneth cell numbers at onset of gastrointestinal graft-versus-host disease identify patients at high risk for nonrelapse mortality. *Blood* **122,** 1505–1509 (2013).
24. Kabiri, Z. *et al.* Stroma provides an intestinal stem cell niche in the absence of epithelial Wnts. *Development* **141,** 2206–2215 (2014).
25. Tian, H. *et al.* A reserve stem cell population in small intestine renders Lgr5-positive cells dispensable. *Nature* **478,** 255–259 (2011).
26. Durand, A. *et al.* Functional intestinal stem cells after Paneth cell ablation induced by the loss of transcription factor Math1 (Atoh1). *Proc. Natl Acad. Sci. USA* **109,** 8965–8970 (2012).
27. Couturier, M. *et al.* IL-22 deficiency in donor T cells attenuates murine acute graft-versus-host disease mortality while sparing the graft-versus-leukemia effect. *Leukemia* **27,** 1527–1537 (2013).
28. Zhao, K. *et al.* Interleukin-22 aggravates murine acute graft-versus-host disease by expanding effector T cell and reducing regulatory T cell. *J. Interferon Cytokine Res.* **34,** 707–715 (2014).
29. Munneke, J. M. *et al.* Activated innate lymphoid cells are associated with a reduced susceptibility to graft-versus-host disease. *Blood* **124,** 812–821 (2014).
30. Hill, G. R. & Ferrara, J. L. The primacy of the gastrointestinal tract as a target organ of acute graft-versus-host disease: rationale for the use of cytokine shields in allogeneic bone marrow transplantation. *Blood* **95,** 2754–2759 (2000).

Supplementary Information is available in the online version of the paper.

Acknowledgements We gratefully acknowledge the technical assistance of the MSKCC Research Animal Resource Center and Molecular Cytology Core Facility. We also thank H. Clevers, H. Farin, S. Middendorp, C. Wiegerinck, J. van Es, M. van de Wetering, N. Sasaki, J. Sun and M. Li for their advice and critical evaluation of our work. This research was supported by National Institutes of Health award numbers K08-HL115355 (A.M.H.), R01-HL125571 (A.M.H.), R01-HL069929 (M.R.M.vdB.), R01-AI100288 (M.R.M.vdB.), R01-AI080455 (M.R.M.vdB.), R01-AI101406 (M.R.M.vdB.), P01-CA023766/Project 4 (R. J. O'Reilly/M.R.M.vdB.), K99-CA176376 (J.A.D.) and P30-CA008748 (MSKCC Core Grant). Support was also received from the US National Institute of Allergy and Infectious Diseases (NIAID contract HHSN272200900059C), the European Union (award GC220918, C. Blackburn), The Experimental Therapeutics Center of MSKCC funded by Mr William H. Goodwin and Mrs Alice Goodwin, The Lymphoma Foundation, Alex's Lemonade Stand, The Geoffrey Beene Cancer Research Center at MSKCC, The Susan and Peter Solomon Divisional Genomics Program, MSKCC Cycle for Survival, and The Lucille Castori Center for Microbes, Inflammation & Cancer. T.C. was supported by Innovational Research Incentives Scheme Vidi grant 91710377 from the Netherlands Organization for Scientific Research (Zon-MW), and M.R.-H. was supported by the People Programme (Marie Curie Actions) of the European Union's Seventh Framework Programme FP7/2007-2013 under REA grant agreement no. 289720. A.M.M. was supported by the Bio Medical Exchange Program of the Deutscher Akademischer Austauschdienst. C.A.L. was supported by Dutch Cancer Society clinical fellowship grant 2013-5883 and by a mobility grant from the University Medical Center Utrecht. J.A.D. was supported by a C. J. Martin fellowship from the Australian National Health and Medical Research Council, a Scholar Award from the American Society of Hematology, and the Mechtild Harf Research Grant from the DKMS Foundation for Giving Life. A.M.H. was supported by a Scholar Award from the American Society of Hematology, a New Investigator Award from the American Society for Blood and Marrow Transplantation, and the Amy Strelzer Manasevit Research Program. A provisional patent application has been filed on the use of IL-22 and F-652 as ISC growth factors (US 61/901,151) with A.M.H., C.A.L. and M.R.M.vdB. listed as inventors.

Author Contributions C.A.L. and M.C. designed and performed organoid experiments. A.M.M. and M.H.O. performed and analysed *in vivo* experiments. J.A.D., R.R.J. and E.V. provided input and helped with various assays. L.F.Y., O.M.S. and G.L. performed and monitored bone marrow transplants and maintained the mouse colonies. J.A.I. assisted with organoid quantification. Y.-Y.F. analysed crypt sizes and confocal microscopy. S.T. assisted with ILC co-culture experiments. G.H., M.L.M. and R.K. assisted with ISC isolation and *in vivo* ISC quantification experiments and provided reagents and expertise. K.P.O. and L.D. assisted with adeno-Cre experiments and optimizing various assays. Y.-H.L. and N.F.S. assisted with Paneth cell deficiency experiments. M.M. and E.E.N. performed the GSEA analyses and assisted with reagents and resources. M.R.-H. performed PCR analyses on purified stem cells and immune cells under the guidance of T.C., and C.L. analysed intestinal histopathology. M.R.M.vdB. and A.M.H. supervised the research. All authors contributed to experimental design, interpretation and manuscript editing.

Author Information Reprints and permissions information is available at www.nature.com/reprints. The authors declare no competing financial interests. Readers are welcome to comment on the online version of the paper. Correspondence and requests for materials should be addressed to A.M.H. (hanasha@mskcc.org).

METHODS

Mice. C57BL/6 (B6, H-2^b) and LP (H-2^b) mice were obtained from Jackson Laboratory. B6 Lgr5-LacZ and B6 lgr5-gfp-ires-CreERT2 (Lgr5–GFP) mice were provided by H. Clevers[1,10]. Mouse maintenance and procedures were done in accordance with the institutional protocol guideline of the Memorial Sloan Kettering Cancer Center (MSKCC) Institutional Animal Care and Use Committee. Mice were housed in micro-isolator cages, five per cage, in MSKCC pathogen-free facilities, and received standard chow and autoclaved sterile drinking water. To adjust for differences in weight and intestinal flora among other factors, identical mice were purchased from Jackson and then randomly distributed over different cages and groups by a non-biased technician who had no insight or information about the purpose or details of the experiment. The investigations assessing clinical outcome parameters were performed by non-biased technicians with no particular knowledge or information regarding the hypotheses of the experiments and no knowledge of the specifics of the individual groups.

Crypt isolation and cell dissociation. Isolation of intestinal crypts and the dissociation of cells for flow cytometry analysis were largely performed as previously described[10]. In brief, after euthanizing the mice with CO_2 and collecting small and large intestines, the organs were opened longitudinally and washed with PBS. To dissociate the crypts, small intestine was incubated at 4 °C in EDTA (10 mM) for 15 min and then in EDTA (5 mM) for an additional 15 min. Large intestine was incubated in collagenase type 4 (Worthington) for 30 min at 37 °C to isolate the crypts. To isolate single cells from small and large intestine crypts, the pellet was further incubated in 1× TrypLE express (Gibco, Life Technologies) supplemented with 0.8 kU ml^{-1} DNase1 (Roche).

Organoid culture. For mouse organoids, depending on the experiments, 200–400 crypts per well were suspended in Matrigel composed of 25% advanced DMEM/F12 medium (Gibco) and 75% growth-factor-reduced Matrigel (Corning). After the Matrigel polymerized, complete ENR medium containing advanced DMEM/F12 (Sigma), 2 mM Glutamax (Invitrogen), 10 mM HEPES (Sigma), 100 U ml^{-1} penicillin, 100 μg ml^{-1} streptomycin (Sigma), 1 mM *N*-acetyl cysteine (Sigma), B27 supplement (Invitrogen), N2 supplement (Invitrogen), 50 ng ml^{-1} mouse EGF (Peprotech), 100 ng ml^{-1} mouse Noggin (Peprotech) and 10% human R-spondin-1-conditioned medium from R-spondin-1-transfected HEK 293T cells[31] was added to small intestine crypt cultures[10]. For experiments evaluating organoid budding, the concentration of R-spondin-1 was lowered to 1.25–5%. For mouse large intestine, crypts were cultured in 'WENR' medium containing 50% WNT3a-conditioned medium in addition to the aforementioned proteins and 1% BSA (Sigma), and supplemented with SB202190 (10 μM, Sigma), ALK5 inhibitor A83-01 (500 nM, Tocris Bioscience) and nicotinamide (10 mM, Sigma). Media was replaced every 2–3 days. Along with medium changes, treatment wells received different concentrations of rmIL-22 (Genscript). We also tested the effects of F-652 (Generon Corporation). In some experiments, organoids from crypts were cultured in the presence of Stattic (Tocris Bioscience). For passaging of organoids, after 5–7 days of culture, organoids were passaged by mechanically disrupting with a seropipet and cold media to depolymerize the Matrigel and generate organoid fragments. After washing away the old Matrigel by spinning down at 600 r.p.m., organoid fragments were replated in liquid Matrigel.

ISCs were isolated from Lgr5–GFP mice using a modified crypt isolation protocol with 20 min of 30 mM EDTA[32,33] followed by several strainer steps and a 5-min incubation with TrypLE and 0.8 kU ml^{-1} DNase1 under minute-to-minute vortexing to make a single-cell suspension. The Lgr5–GFP^{high} cells were isolated by FACS. Approximately 5,000 ISCs were plated in 30 μl Matrigel and cultured in WENR media containing Rho-kinase/ROCK inhibitor Y-27632 (10 μM, Tocris Bioscience) and Jagged1 (1 μM, Anaspec). Starting from day 4, ISC were cultured without Wnt.

For lymphocyte co-culture experiments, ILCs were isolated from the small intestine lamina propria. Washed small intestine fragments were incubated in EDTA/IEL solution (1× PBS with 5% FBS, 10 mM HEPES buffer, 1% penicillin/streptomycin (Corning), 1% L-glutamine (Gibco), 1 mM EDTA and 1 mM dithiothreitol (DTT)) in a 37 °C shaker for 15 min. The samples were strained (100 μM) and put in a Collagenase solution (RPMI 1640, 5% FCS, 10 mM HEPES, 1% penicillin/streptomycin, 1% glutamine, 1 mg ml^{-1} collagenase D (Roche) and 1 U ml^{-1} DNase1 (Roche) and incubated twice for 10 min in a 37 °C shaker. Afterwards, the samples were centrifuged at 1,500 r.p.m. for 5 min and washed with RPMI solution without enzymes. After several washes, the cell suspension was transferred into a 40% Percoll solution (in PBS), which is overlaid on an 80% Percoll solution. After spinning the interface containing the lamina propria, mononuclear cells was aspirated and washed in medium. The cell suspension was then stained with extracellular markers and Topro3 for viability. Topro3$^-$CD45$^+$CD11b$^-$CD11c$^-$CD90$^+$ LPLs from B6 wild-type and *Il22*$^{-/-}$ mice and Topro3$^-$CD45$^+$CD3$^-$RORγt$^+$ ILC3s[34] from Rorc(γt)-GFP$^+$ mice (Jackson) were sorted for co-cultures with SI crypts. (For antibodies used, see Supplementary Table 1.) To activate and maintain LPLs and ILCs in culture, rmIL-2 (1,000 U ml^{-1}), rmIL-15 (10 ng ml^{-1}), rmIL-7 (50 ng ml^{-1}) and rmIL-23 (50 ng ml^{-1}) were added to the ENR medium in co-culture experiments. We have also performed co-cultures with addition of only rmIL-23 (50 ng ml^{-1}) to ENR media. LPLs and SI crypts were cultured in Matrigel with a 7:1 LPL:crypt ratio; ILCs and crypts were cultured in Matrigel with a 25:1 ILC:crypt ratio. Co-cultures were compared to crypts cultured in ENR plus cytokines without LPLs or ILCs present. A neutralizing monoclonal antibody against IL-22 (8E11, Genentech)[35] was used to abrogate IL-22-specific effects of ILCs.

For specific experiments, organoids were cultured from fresh crypts obtained from specific genetically modified mice, such as the *Stat1*$^{-/-}$ mice (129S6/SvEv-Stat1tm1Rds, Taconic) and *Stat3*$^{fl/fl}$ mice (Jackson). Organoids from *Stat3*$^{fl/fl}$ mice that had been grown for 7 days were dissociated as single cells and incubated with adenoviral-Cre (University of Iowa) to cause the deletion of *Stat3* from floxed organoid cells. Frozen passaged organoids from *Lgr5*^{DTR} (Lgr5-DTR)[25] mice were used to culture organoids in which Lgr5$^+$ stem cells could be depleted with daily administration of diphtheria toxin (1 ng μl^{-1}) .

For Paneth-cell-deficient organoid cultures, frozen crypts from *Atoh1*$^{\Delta IEC}$ mice[36] depleted of Paneth cells were used to culture organoids. As previously described[36], *Atoh1*$^{\Delta IEC}$ mice (and littermate controls) were given an intraperitoneal injection of tamoxifen (1 mg per mouse, Sigma, dissolved in corn oil) for 5 consecutive days to achieve deletion of ATOH1 from intestinal epithelium. Animals were euthanized on day 7 after the first injection, and intestinal crypts were isolated and frozen in 10% dimethylsulfoxide (DMSO) and 90% FBS.

To investigate the effect of IL-22 on human small intestine, we generated human duodenal organoids from banked frozen organoids (>passage 7) that had been previously generated from biopsies obtained during duodenoscopy of three independent healthy human donors. All human donors had been investigated for coeliac disease, but turned out to have normal pathology. All provided written informed consent to participate in this study according to a protocol reviewed and approved by the review board of the UMC Utrecht, The Netherlands (protocol STEM study, METC 10-402/K). Human organoids were cultured in 10 μl Matrigel drops in expansion medium containing WENR with 10 nM SB202190, 500 nM A83-01 and 10 mM nicotinamide. For IL-22 stimulation experiments, rhIL-22 10 ng ml^{-1} (Genscript) was added daily. For the purpose of size measurements at day 6, organoids were passaged as single cells.

Where applicable, organoid cultures were performed using conditioned media containing R-spondin-1 and WNT3a produced by stably transfected cell lines. R-spondin-1-transfected HEK293T cells[31] were provided by C. Kuo. WNT3a-transfected HEK293T cells were provided by H. Clevers (patent WO2010090513A2). Cell lines were tested for mycoplasma and confirmed to be negative.

Organoid measurement. For size evaluation, the surface area of organoid horizontal cross sections was measured. If all organoids in a well could not be measured, several random non-overlapping pictures were acquired from each well using a Zeiss Axio Observer Z1 inverted microscope and then analysed using MetaMorph or ImageJ software. Organoid perimeters for area measurements have been defined manually and by automated determination using the Analyze Particle function of ImageJ software, with investigator verification of the automated determinations, as automated measurements allowed for unbiased analyses of increased numbers of organoids. For automated size measurements, the threshold for organoid identification was set based on monochrome images. The sizes of the largest and smallest organoids in the reference well were measured manually, and their areas were used as the reference values for setting the minimal and maximal particle sizes. Organoids touching the edge of the images were excluded from the counting. After 5–7 days in culture, total organoid numbers per well were counted by light microscopy to evaluate growth efficiency. All organoid numbers were counted manually in this fashion except for the organoid counts presented in Extended Data Fig. 5b, which were counted using automated ImageJ analysis, as these organoids were too numerous to count manually. To compare organoid efficiency in different conditions, combining experiments with different organoid numbers, the percentage of organoids relative to the number of organoids in ENR-control (rmIL-22 0 ng ml^{-1}) was calculated. The efficiency from sorted ISCs was presented as the percentage of cells forming organoids per number of seeded cells.

BMT. BMT procedures were performed as previously described[37]. A minor histocompatibility antigen-mismatched BMT model (LP into B6; H-2^b into H-2^b) was used. Female B6 wild-type mice were typically used as recipients for transplantation at an age of 8–10 weeks. Recipient mice received 1,100 cGy of split-dosed lethal irradiation (550 cGy × 2) 3–4 h apart to reduce gastrointestinal toxicity. To obtain LP bone marrow cells from euthanized donor mice, the femurs and tibias were collected aseptically and the bone marrow canals washed out with sterile media. Bone marrow cells were depleted of T cells by incubation with

anti-Thy 1.2 and low-TOX-M rabbit complement (Cedarlane Laboratories). The TCD bone marrow was analysed for purity by quantification of the remaining T cell contamination using flow cytometry. T cell contamination was usually about 0.2% of all leukocytes after a single round of complement depletion. LP donor T cells were prepared by collecting splenocytes aseptically from euthanized donor mice. T cells were purified using positive selection with CD5 magnetic Microbeads with the MACS system (Miltenyi Biotec). T cell purity was determined by flow cytometry, and was routinely approximately 90%. Recipients typically received 5×10^6 TCD bone marrow cells with or without 4×10^6 T cells per mouse via tail vein injection.

Mice were monitored daily for survival and weekly for GVHD scores with an established clinical GVHD scoring system (including weight, posture, activity, fur ruffling and skin integrity) as previously described[38]. A clinical GVHD index with a maximum possible score of ten was then generated. Mice with a score of five or greater were considered moribund and euthanized by CO_2 asphyxia.

***In vivo* cytokine administration.** Recombinant mouse IL-22 was purchased from GenScript and reconstituted as described by the manufacturer to a concentration of 40 μg ml^{-1} in PBS. Mice were treated daily via i.p. injection with either 100 μl PBS or 100 μl PBS containing 4 μg rmIL-22. IL-22 administration was started on day 7 after BMT. This schedule was based on the results of rmIL-22 pharmacokinetics tested in untransplanted mice. For *in vivo* F-652 administration, starting from day 7 after BMT, mice were injected subcutaneously every other day for ten consecutive weeks with PBS or 100 μg kg^{-1} F-652.

Histopathology analysis of GVHD target organs. Mice were euthanized for organ analysis 21 days after BMT using CO_2 asphyxiation. For histopathological analysis of GVHD, the small and large intestines were formalin-preserved, paraffin-embedded, sectioned and stained with haematoxylin and eosin. An expert in the field of GVHD pathology, blinded to allocation, assessed the sections for markers of GVHD histopathology. As described previously[38], a semiquantitative score consisting of 19 different parameters associated with GVHD was calculated.

LacZ staining. For evaluation of stem-cell numbers, small intestines from Lgr5-LacZ recipient mice that were transplanted with LP bone marrow (and T cells where applicable) were collected. β-galactosidase (LacZ) staining was performed as previously described previously[1]. Washed 2.5-cm-sized small intestine fragments were incubated with an ice-cold fixative, consisting of 1% formaldehyde, 0.2% NP40 and 0.2% gluteraldehyde. After removing the fixative, organs were stained for the presence of LacZ according to manufacturer's protocol (LacZ staining kit, Invivogen). The organs were then formalin-preserved, paraffin-embedded, sectioned and counterstained with Nuclear Fast Red (Vector Labs).

Immunohistochemistry staining. Immunohistochemistry detection of REG3β was performed at the Molecular Cytology Core Facility of MSKCC using a Discovery XT processor (Ventana Medical Systems). Formalin-fixed tissue sections were deparaffinized with EZPrep buffer (Ventana Medical Systems), antigen retrieval was performed with CC1 buffer (Ventana Medical Systems) and sections were blocked for 30 min with Background Buster solution (Innovex). Slides were incubated with anti-REG3β antibodies (R&D Systems, MAB5110; 1 μg ml^{-1}) or isotype (5 μg ml^{-1}) for 6 h, followed by a 60-min incubation with biotinylated goat anti-rat IgG (Vector Laboratories, PK-4004) at a 1:200 dilution. The detection was performed with a DAB detection kit (Ventana Medical Systems) according to the manufacturer's instructions. Slides were counterstained with haematoxylin (Ventana Medical Systems), and coverslips were added with Permount (Fisher Scientific). See Supplementary Table 1 for full description of antibodies used.

Immunofluorescent staining and microscopic imaging. Immunofluorescent staining was performed at the Molecular Cytology Core Facility of Memorial Sloan Kettering Cancer Center using a Discovery XT processor (Ventana Medical Systems). Formalin-fixed tissue sections were deparaffinized with EZPrep buffer (Ventana Medical Systems), and antigen retrieval was performed with CC1 buffer (Ventana Medical Systems). Sections were blocked for 30 min with Background Buster solution (Innovex) followed by avidin/biotin blocking for 12 min. IL-22R antibodies (R&D Systems, MAB42; 0.1 μg ml^{-1}) were applied and sections were incubated for 5 h followed by 60 min incubation with biotinylated goat anti-rat IgG (Vector Laboratories, PK-4004) at a 1:200 dilution. The detection was performed with streptavidin–horseradish peroxidase (HRP) D (part of DABMap kit, Ventana Medical Systems), followed by incubation with Tyramide Alexa Fluor 488 (Invitrogen, T20932) prepared according to manufacturer's instruction with predetermined dilutions. Next, lysozyme antibodies (DAKO, A099; 2 μg ml^{-1}) were applied and sections were incubated for 6 h followed by incubation with biotinylated goat anti-rabbit IgG (Vector Laboratories, PK6101) for 60 min. The detection was performed with streptavidin–HRP D (part of DABMap kit, Ventana Medical Systems), followed by incubation with Tyramide Alexa Fluor 594 (Invitrogen, T20935) prepared according to manufacturer's instruction with predetermined dilutions. Finally, GFP antibodies were applied and sections were incubated for 5 h followed by incubation with biotinylated goat anti-chicken IgG (Vector Laboratories, BA-9010) for 60 min. The detection was performed with streptavidin–HRP D (part of DABMap kit, Ventana Medical Systems), followed by incubation with Tyramide Alexa Fluor 647 (Invitrogen, T20936) prepared according to manufacturer instruction with predetermined dilutions. Slides were counterstained with DAPI (Sigma Aldrich, D9542; 5 μg ml^{-1}) for 10 min and coverslips were added with Mowiol. For immunofluorescent and other microscopic imaging, including LacZ and immunohistochemistry slides, contrast and white balance were set based on control slides for each experiment, and the same settings were used for all slides to maximize sharpness and contrast. See Supplementary Table 1 for full description of antibodies used.

Cytokine multiplex assay. Spleen and small intestine were collected from euthanized BMT recipients, and organs were then homogenized and spun down. The supernatant was stored at −20 °C until use for cytokine analysis. The cytokine multiplex assays were performed on thawed samples with the mouse Th1/Th2/Th17/Th22 13plex (FlowCytomix Multiplex kit, eBioscience) and performed according to the manufacturer's protocol.

Flow cytometry. For *in vivo* experiments, lymphoid organs were collected from euthanized mice and processed into single cell suspension. Cells were stained with the appropriate mixture of antibodies. For intracellular analysis, an eBioscience Fixation/Permeabilization kit was used per the manufacturer's protocol. After thorough washing, the cells were stained with intracellular and extracellular antibodies simultaneously. Fluorochrome-labelled antibodies were purchased from BD Pharmingen (CD4, CD8, CD24, CD25, CD45, α4β7 and P-STAT3 Y705, P-STAT1 Y701), eBioscience (FOXP3), R&D (IL-22R), and Invitrogen (GFP). DAPI and Fixable Live/Dead Cell Stain Kits (Invitrogen) were used for viability staining. Paneth cells were identified based on bright CD24 staining and side scatter granularity as described previously[2].

For flow cytometry of small intestine organoid cells, organoids were dissociated using TrypLE (37 °C). After vigorously pipetting through a p200 pipette causing mechanical disruption, the crypt suspension was washed with 10 ml of DMEM/F12 medium containing 10% FBS and 0.8 kU ml^{-1} DNase1 and passaged through a cell strainer. Where applicable, the cells were directly stained or first fixed (4% paraformaldehyde) and permeabilized (methanol) depending on the extracellular or intracellular location of the target protein. All stainings with live cells were performed in PBS without Mg^{2+} and Ca^{2+} with 0.5% BSA. For EdU incorporation experiments there was a 1 h pre-incubation of EdU in the ENR medium of the intact organoid cultures before dissociating the cells with TrypLE. Cells were stained using Click-it kits for imaging and flow cytometry (Life Technologies). For cell cycle analysis, single cell suspensions obtained from dissociated organoids were fixed and stained with Hoechst 33342 (Life Technologies), then assessed with flow cytometry for DNA content and ploidy.

For intracellular pSTAT staining of organoids, organoids were mechanically disrupted into crypt fragments, stimulated for 20 min with 20 ng ml^{-1} IL-22 at 37 °C, and then fixed with 4% paraformaldehyde (10 min at 37 °C). To assess STAT activation in Lgr5$^+$ cells, after freshly isolating crypts from Lgr5–GFP mice, single-cell suspensions including Y-27632 (10 μM) were stimulated with IL-22. After obtaining a single cell suspension of stimulated and fixed cells, the samples were filtered (40 μM) and permeabilized with ice-cold (−20 °C) methanol. Fixed and permeabilized cells were rehydrated with PBS and thoroughly washed with PBS before staining, then stained with anti-phospho-STAT3 and anti-phospho-STAT1, plus anti-GFP or cell surface markers, for 30 min at 4 °C.

All flow cytometry was performed with an LSRII cytometer (BD Biosciences) using FACSDiva (BD Biosciences), and the data were analysed with FlowJo software (Treestar). See Supplementary Table 1 for full description of antibodies used.

Immunoblotting analysis. Western blot analysis was carried out on total protein extracts. Free-floating crypts isolated from small intestine were treated in DMEM supplemented with Y-27632 (10 ng ml^{-1}, Tocris) and IL-22 (5 ng ml^{-1}, 30 min). Vehicle (PBS) was added to control wells. Crypts were then lysed in RIPA buffer containing a cocktail of protease and phosphatase inhibitors (Sigma). After sonication, protein amount was determined using the bicinchoninic acid assay Kit (Pierce). Loading 30 μg per lane of lysate, proteins were separated using electrophoresis in a 10% polyacrylamide gel and transferred to nitrocellulose. Membranes were blocked for 1 h at room temperature with 1% Blot-Qualified BSA (Promega, W384A) and 1% non-fat milk (LabScientific, M0841) and then incubated overnight at 4 °C with the following primary antibodies: rabbit anti-phospho-STAT1 (7649P), rabbit anti-phospho-STAT3 (9131S), rabbit anti-STAT1 (9172P) and rabbit anti-STAT3 (4904P), all from Cell Signaling. This was followed by incubation with the secondary antibody anti-rabbit HRP (7074P2) and visualization with the Pierce ECL Western Blotting Substrate (Thermo Scientific, 32106).

MTT assay. Cell viability in organoids was assessed with a 3-(4,5-dimethylthiazol-2-yl)-2,5-diphenyltetrazolium (MTT) test, based on the identification of

metabolically active cells. The organoids were incubated with MTT (0.9 mg ml^{-1} final concentration, Sigma) for 2 h at 37 °C. Matrigel and cells containing intracellular reduction end product formazan were solubilized with acidic isopropanol (isopropanol with HCl) and the reduction end formazan production was evaluated by spectrophotometry using the Infinite M1000 pro plate reader (Tecan).

RT–qPCR. For qPCR, segments of small intestine or isolated crypts were collected from euthanized mice and stored at −80 °C. Alternatively, RNA was isolated from organoids after *in vitro* culture. Extracted RNA was also stored at −80 °C. Reverse transcriptase PCR (RT–PCR) was performed with a QuantiTect Reverse Transcription Kit (QIAGEN) or a High-Capacity RNA-to-cDNA Kit (Applied Biosystems). qPCR was performed on a Step-One Plus or QuantStudio 7 Flex System (Applied Biosystems) using TaqMan Universal PCR Master Mix (Applied Biosystems). Specific primers were obtained from Applied Biosystems: *Actb*: Mm01205647_g1; *Hprt*: Mm00446968_m1; *Reg3b*: Mm00440616_g1; *Reg3g*: Mm00441127_m1; *Wnt3*: Mm00437336_m1; *Egf*: Mm00438696_m1; *Rspo3*: Mm00661105_m1; *Axin2*: Mm00443610_m1; *Ctnnb1*: Mm00483039_m1; *Defa1*: Mm02524428_g1; and *Il22ra1*: Mm01192943_m1. Other primers were obtained from PrimerBank: *Gapdh* (ID 6679937a1), *Cdkn1a* (also known as *p21*) (ID 6671726a1); *Cdkn2d* (also known as *p19*) (ID 31981844a1); *Wnt3a* (ID 7106447a1); *Axin2* (ID 31982733a1); *Hes1* (ID 6680205a1) *Dll4* (ID 9506547a1) *Dll1* (ID 6681197a1), for which cDNAs were amplified with SYBR master mix (Applied Biosystems) in QuantStudio 7 Flex System (Applied Biosystems). Relative amounts of mRNA were calculated by the comparative ΔC_t method with *Actb*, *Hprt* or *Gapdh* as house-keeping genes.

For *Il22ra1* qPCR on Lgr5$^+$ cells, dissociated crypt cells from Lgr5–GFP mice were stained and isolated using the following monoclonal antibodies/parameters: EpCAM-1 (G8.8; BD Bioscience); CD45 (30F11; Life Technologies); CD31 (390; BioLegend), Ter119 (Ter119; BioLegend); GFP expression; dead cells were excluded using 7AAD. Cells were acquired on a BD ARIAIII and FACS-sorted. Cells were sorted directly into RA-1/TCEP (Macherey-Nagel) lysis buffer and stored at −80 °C until further analysis. RNA of haematopoietic cells (composite of dendritic cells, ILCs and B cells) was used as negative control. RNA was extracted using the NucleoSpin RNA XS kit (Machery Nagel) and cDNA was prepared with Ovation Pico and PicoSL WTA Systems V2 (NuGen). For qPCR, a Neviti Thermal Cycler (Applied Biosystems) and DyNAmo Flash SYBR Green qPCR kit (Finnzymes) were used, with the addition of $MgCl_2$ to a final concentration of 4 mM. All reactions were done in duplicate and normalized to *Gapdh*. Relative expression was calculated by the cycling threshold (C_t) method as $2^{-\Delta Ct}$. The primer sequences were as follows: *Il22ra1*: forward 5′-TCGGCTTGCTCTGTTATC-3′, reverse 5′-CCACTGAGGTCCAAGACA-3′.

GSEA. To explore the association of ISC gene signatures (GSE33948 and GSE23672)[16] with STAT3-regulated genes, we performed GSEA in a mouse DSS colitis data set (GSE15955)[12], comparing *Stat3*$^{fl/fl}$*;Villin-Cre*$^-$ (wild type) and *Stat3*$^{fl/fl}$*;Villin-Cre*$^+$ (*Stat3*$^{\Delta IEC}$) mice with DSS colitis (GSEA2-2.2.0; http://www.broadinstitute.org/gsea)[39,40]. A Paneth cell signature gene set was used as a negative control (DLL1$^+$CD24^{hi}, GSE39915)[17]. Nominal *P* values are shown.

Statistics and software. No statistical methods were used to predetermine sample size. To detect an effect size of >50% difference in means, with an assumed coefficient of variation of 30%, common in biological systems, we attempted to have at least five samples per group, particularly for *in vivo* studies. All experiments were repeated at least once. No mice were excluded from experiments. Experiments that were technical failures, such as experiments *in vitro* where cultures did not grow or experiments *in vivo* where transplanted control mice (bone marrow plus T cells) did not develop GVHD, were not included for analysis. Occasional individual mice that died post-transplant before analysis could not be included for tissue evaluation.

All data are mean and s.e.m. for the various groups. Statistics are based on '*n*' biological replicates. All tests performed are two sided. For the comparisons of two groups, a *t*-test or non-parametric test was performed. Adjustments for multiple comparisons were made. In most cases, non-parametric testing was performed if normal distribution could not be assumed. RT–qPCR reactions and ordinal outcome variables were tested non-parametrically. All analyses of statistical significance were calculated and displayed compared with the reference control group unless otherwise stated.

There is large biological variation in organoid size. Statistical analyses of organoid sizes were thus based on all evaluable organoids (at least 25 organoids per group for all experiments). Statistical analyses of organoid numbers and efficiency were based on individual wells. To take into account intra-individual and intra-experimental variation as well, all *in vitro* experiments were performed at least twice with several wells per condition, and sample material coming from at least two different mice. Statistical analyses of stem-cell numbers (Lgr5-LacZ mice) *in vivo* were performed on several independent sections from multiple mice. Statistics were calculated and display graphs were generated using Graphpad Prism.

31. Ootani, A. *et al.* Sustained *in vitro* intestinal epithelial culture within a Wnt-dependent stem cell niche. *Nature Med.* **15,** 701–706 (2009).
32. Wang, F. *et al.* Isolation and characterization of intestinal stem cells based on surface marker combinations and colony-formation assay. *Gastroenterology* **145,** 383–395 (2013).
33. Magness, S. T. *et al.* A multicenter study to standardize reporting and analyses of fluorescence-activated cell-sorted murine intestinal epithelial cells. *Am. J. Physiol. Gastrointest. Liver Physiol.* **305,** G542–G551 (2013).
34. Spits, H. *et al.* Innate lymphoid cells—a proposal for uniform nomenclature. *Nature Rev. Immunol.* **13,** 145–149 (2013).
35. Zheng, Y. *et al.* Interleukin-22 mediates early host defense against attaching and effacing bacterial pathogens. *Nature Med.* **14,** 282–289 (2008).
36. Shroyer, N. F. *et al.* Intestine-specific ablation of mouse atonal homolog 1 (Math1) reveals a role in cellular homeostasis. *Gastroenterology* **132,** 2478–2488 (2007).
37. Alpdogan, Ö. *et al.* IL-7 enhances peripheral T cell reconstitution after allogeneic hematopoietic stem cell transplantation. *J. Clin. Invest.* **112,** 1095–1107 (2003).
38. Cooke, K. R. *et al.* An experimental model of idiopathic pneumonia syndrome after bone marrow transplantation: I. The roles of minor H antigens and endotoxin. *Blood* **88,** 3230–3239 (1996).
39. Subramanian, A. *et al.* Gene set enrichment analysis: a knowledge-based approach for interpreting genome-wide expression profiles. *Proc. Natl Acad. Sci. USA* **102,** 15545–15550 (2005).
40. Mootha, V. K. *et al.* PGC-1α-responsive genes involved in oxidative phosphorylation are coordinately downregulated in human diabetes. *Nature Genet.* **34,** 267–273 (2003).

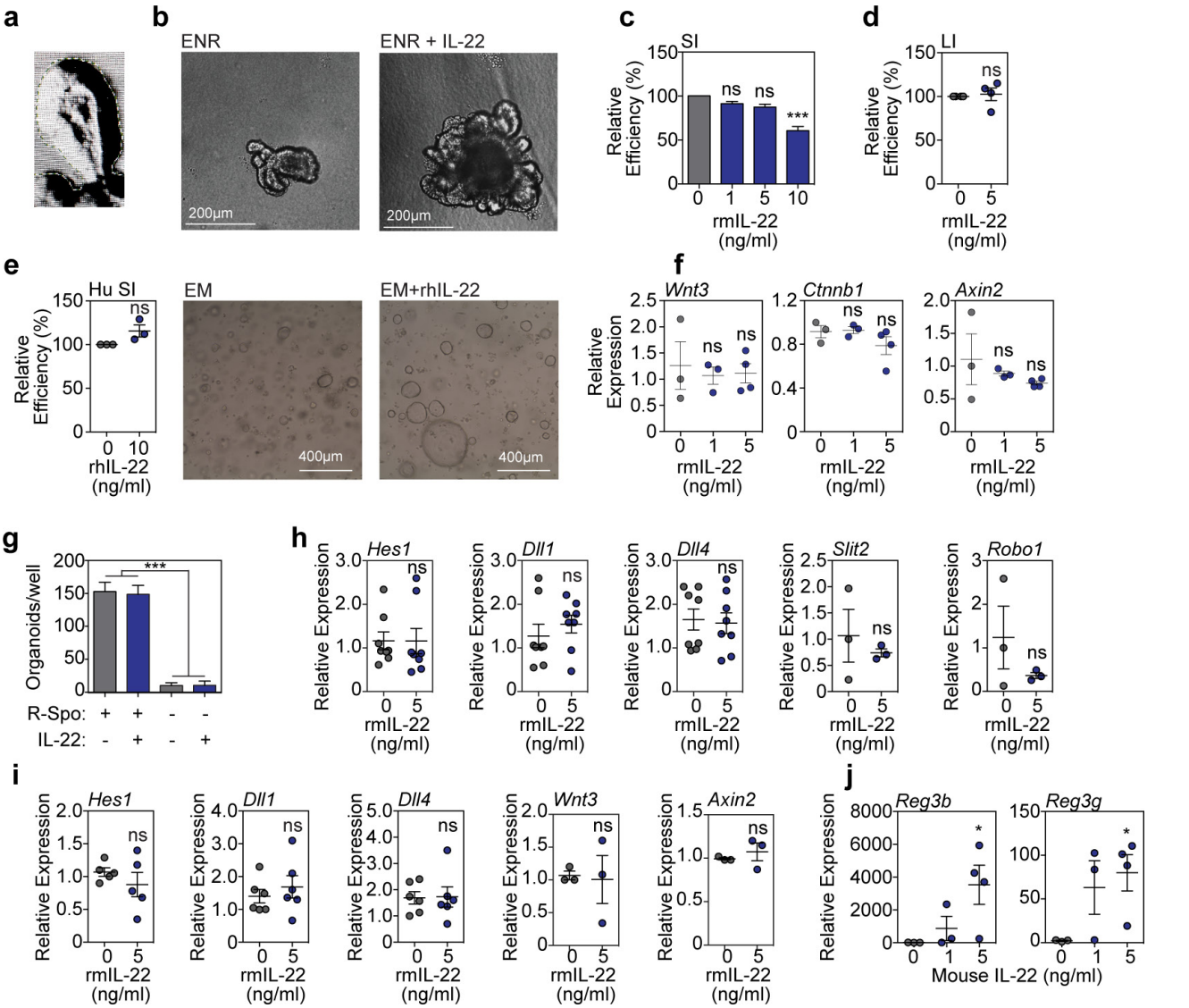

Extended Data Figure 1 | IL-22 increases organoid growth without activating the Wnt or Notch pathways. a, Microscopic tracing of organoid to measure surface area. **b**, Brightfield images of SI organoids from B6 mice, after 7 days of culture with/without IL-22 (5 ng ml^{-1}). **c**–**e**, Organoid efficiency (percentage) relative to control (0 ng ml^{-1}) for B6 SI organoids (statistics on data combined from $n = 19$ wells per group from 19 individual mice) (**c**), B6 large intestine organoids ($n = 4$ mice per group) cultured with/without rmIL-22 for 7 days (**d**), and human SI organoids cultured with/without rhIL-22 for 6 days ($n = 3$ donors per group) (**e**). **f**, RT–qPCR of relative mRNA expression of *Wnt3*, *Ctnnb1* and *Axin2* genes of the Wnt/β-catenin axis in SI organoids cultured with/without rmIL-22; $n = 3$ (0–1 ng ml^{-1}) and $n = 4$ (5 ng ml^{-1}) mice per group. **g**, Numbers of SI organoids per well with/without rmIL-22 (5 ng ml^{-1}) in the presence or absence of R-spondin-1 ($n = 6$ wells per group). **h**, RT–qPCR-determined relative mRNA expression of Notch pathway genes (*Hes1*, *Dll1* and *Dll4*; $n = 8$ mice per group) as well as of *Slit2* and its receptor *Robo1* ($n = 3$ mice per group) in day-7 SI organoids cultured with/without rmIL-22. **i**, Relative expression of *Wnt3* and *Axin2* ($n = 3$ mice per group), *Hes1* ($n = 5$ mice per group), and *Dll1* and *Dll4* ($n = 6$ mice per group) genes in large intestine organoids. **j**, RT–qPCR for the relative mRNA expression of *Reg3b* and *Reg3g* innate antimicrobials in SI organoids cultured with rmIL-22; $n = 3$ (0–1 ng ml^{-1}) and $n = 4$ (5 ng ml^{-1}) mice per group. Organoid efficiency and number comparisons were performed with *t*-tests (two groups) or ANOVA (multiple groups). RT–qPCR statistics were performed with non-parametric Mann–Whitney *U* (two groups) or Kruskal–Wallis (multiple groups) tests. Data are mean and s.e.m.; $*P < 0.05$, $***P < 0.001$. Data combined from at least two independent experiments unless otherwise stated.

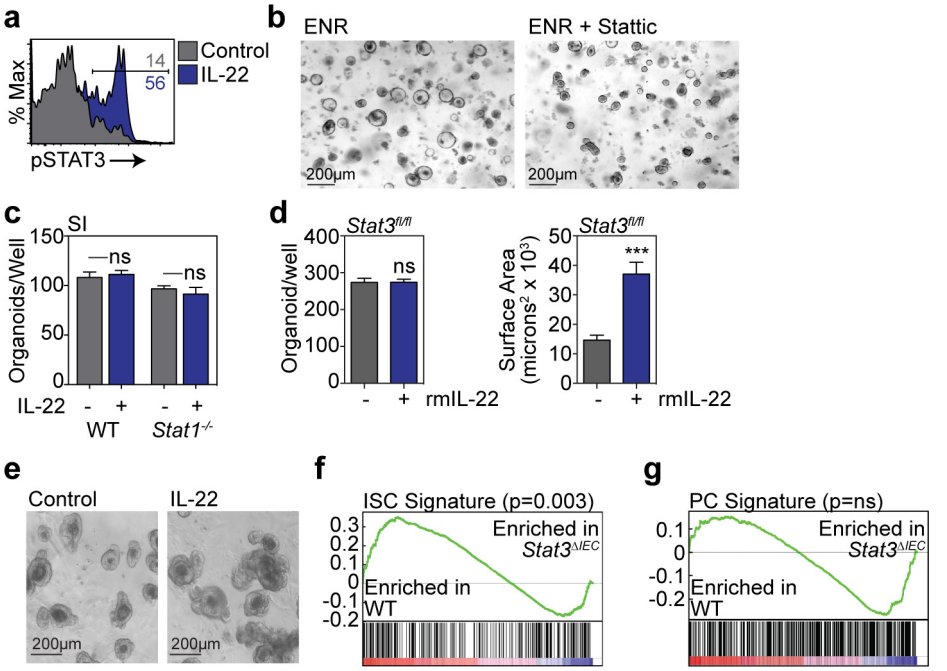

Extended Data Figure 2 | IL-22 activates STAT3 in intestinal organoids, and STAT3 deficiency leads to ISC gene signature loss in mice with colitis. a, Intracellular staining of pSTAT3 (Y705) in organoid cells cultured under standard ENR conditions followed by a 20 min pulse of 20 ng ml^{-1} IL-22, evaluated by flow cytometry; data representative of two independent experiments. **b**, Brightfield images of SI organoids 4 days after crypt culture with/without Stattic; data representative of three experiments. **c**, SI organoids per well from wild-type and *Stat1*$^{-/-}$ mice with/without rmIL-22; $n = 6$ wells per group; ANOVA. **d**, **e**, Day 5 organoids from *Stat3*$^{fl/fl}$ SI crypt cells cultured with/without rmIL-22 (5 ng ml^{-1}) in the absence of adeno-Cre infection; numbers per well ($n = 6$ wells per group) and size ($n = 35$ control and $n = 42$ IL-22-treated organoids per group), *t*-test (**d**); brightfield images representative of three experiments (**e**). **f**, **g**, GSEAs of the expression of a second independent ISC signature gene set (GSE36497) (**f**) and a negative control DLL1^{+}CD24^{hi} Paneth cell (PC) gene set (GSE39915) (**g**) in *Stat3*$^{fl/fl}$; *Villin-Cre*$^{-}$ (wild type) versus *Stat3*$^{fl/fl}$;*Villin-Cre*$^{+}$ (*Stat3*$^{\Delta IEC}$) mice with DSS colitis, using GEO database array data (GSE15955). Each GSEA represents one analysis; nominal *P* values are shown. Data are mean and s.e.m.; ***$P < 0.001$. Data combined from at least two independent experiments unless otherwise stated.

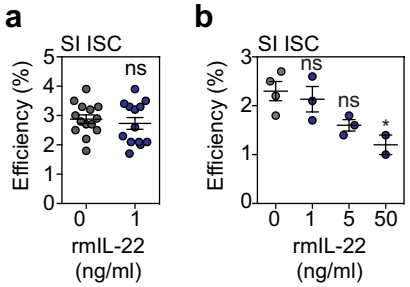

Extended Data Figure 3 | Efficiency of organoid formation from purified ISCs cultured with IL-22. a, **b**, Organoid efficiency as percentage of plated cells, in organoid cultures from sorted Lgr5^{+} ISCs from B6 Lgr5–GFP reporter mice using a concentration of 1 ng ml^{-1} ($n = 14$ wells per group combined from three experiments; *t*-test) (**a**) and with a concentration range (one experiment, $n = 3$ wells per group; ANOVA) (**b**). Data are mean and s.e.m.; $^{*}P < 0.05$.

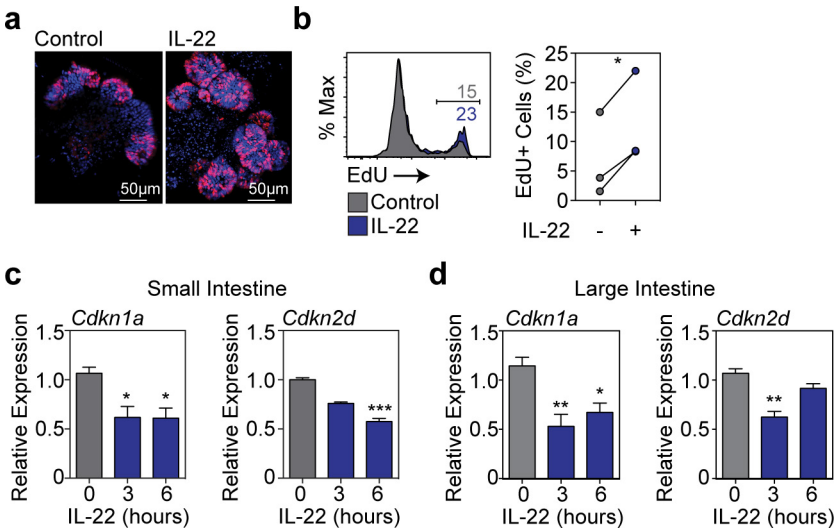

Extended Data Figure 4 | IL-22 increases cellular proliferation in intestinal organoids. a, **b**, Confocal images (nuclear staining, blue; and EdU staining, red; one experiment) (**a**) and FACS analysis (**b**) of EdU incorporation (1 h) in SI organoids cultured in the presence or absence of rmIL-22 (1 ng ml^{-1}); histogram representative of two experiments, graph shows paired *t*-test, $n = 3$ mice per group combined from two experiments. **c**, **d**, *Cdkn1a* and *Cdkn2d* mRNA expression (RT–qPCR) in organoids cultured from small (**c**) and large (**d**) intestine crypts for 24 h with 0, 3 or 6 h exposure to IL-22 before collection; Kruskal–Wallis analysis, $n = 6$ mice per group combined from two independent experiments. Data are mean and s.e.m.; $^{*}P < 0.05$, $^{**}P < 0.01$, $^{***}P < 0.001$.

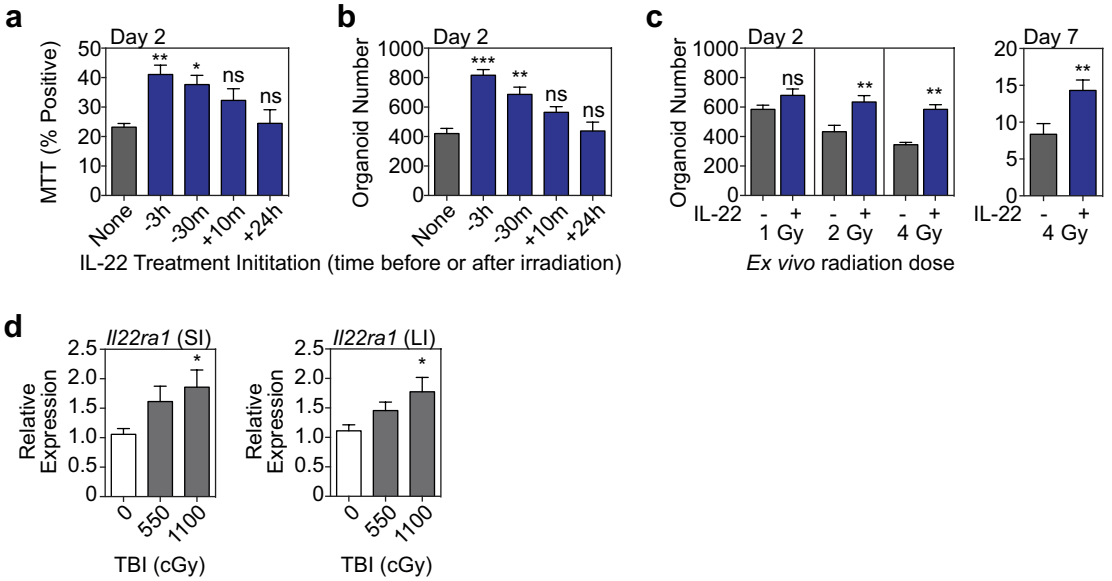

Extended Data Figure 5 | Intestinal organoids and crypts after irradiation. a–c, Dissociated single cells from wild-type B6 crypts were exposed to escalating doses of irradiation *ex vivo*. **a**, **b**, Crypt cells were plated 3 h before irradiation, and cultures were treated with rmIL-22 (5 ng ml^{-1}) added to the culture at 3 h before, 30 min before, 10 min after or 24 h after 4 Gy irradiation. Two days after irradiation, organoids were evaluated for MTT viability testing (percentage positive, $n = 6$ wells per group) (**a**) and the number of organoids generated ($n = 6$ wells per group) (**b**). **c**, The effect of IL-22 after irradiation was evaluated by measuring number of organoids 2 days and 7 days after irradiation (day 2: $n = 9$ wells per group for 1–2 Gy and $n = 6$ wells per group for 4 Gy; day 7: 4 Gy, $n = 20$ wells per group). Culture with/without IL-22 was initiated 3 h before irradiation. **d**, Small and large intestine crypt *Il22ra1* expression determined by qPCR; RNA isolated from fresh crypts of B6 mice collected 1 day (20–26 h) after total body irradiation; $n = 12$ control and $n = 11$ irradiated mice per group. Comparisons performed with *t*-tests (two groups) or ANOVA (multiple groups). Data are mean and s.e.m.; $^*P < 0.05$, $^{**}P < 0.01$, $^{***}P < 0.001$. Data combined from at least two independent experiments.

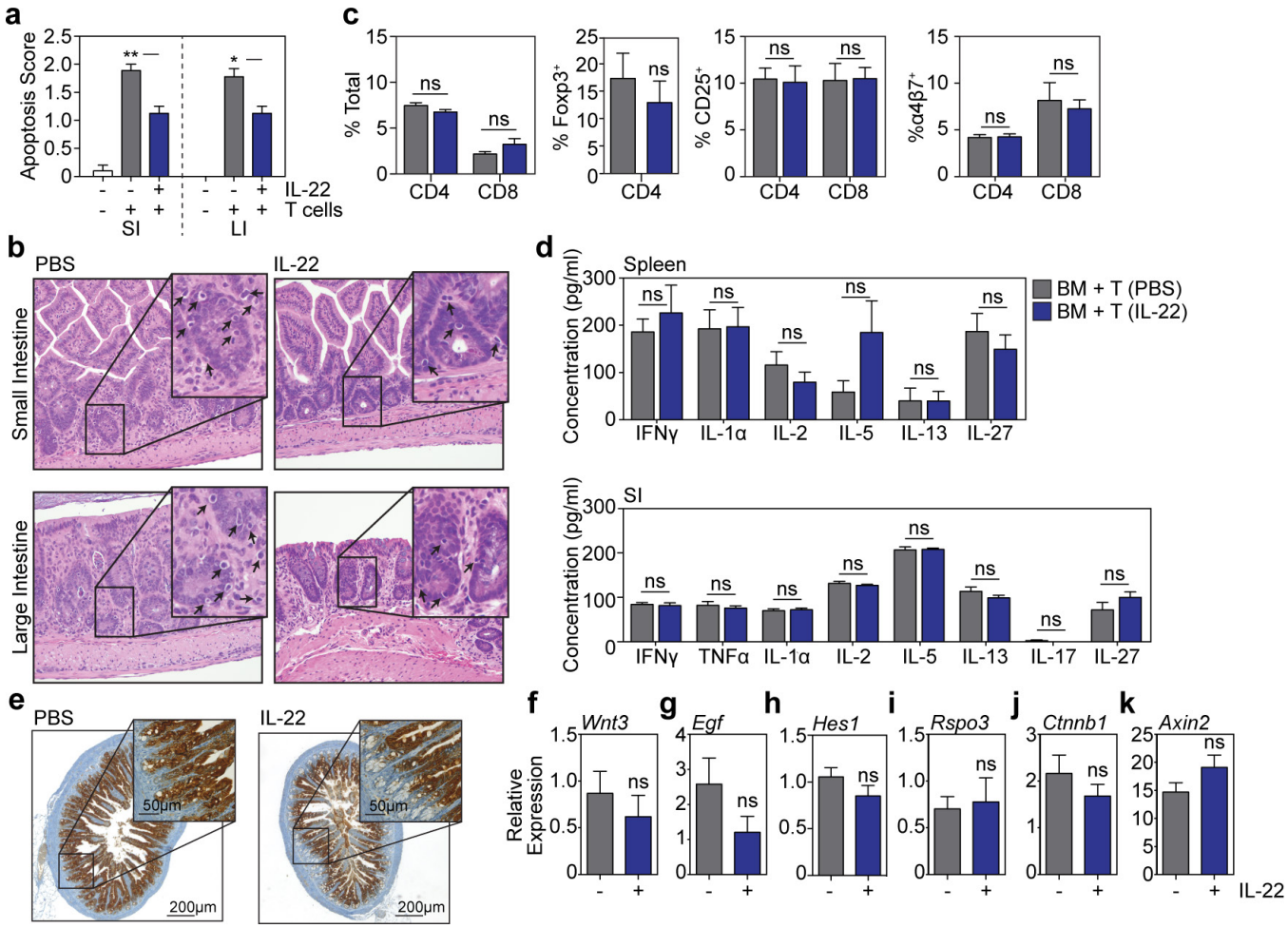

Extended Data Figure 6 | IL-22 treatment after allogeneic BMT. B6 recipient mice were transplanted with only TCD bone marrow from LP donors, or with bone marrow and T cells from LP donors to induce GVHD (H-2^b into H-2^b). Mice receiving T cells were treated daily with PBS or 4 μg rmIL-22 by i.p. injection starting 7 days after BMT. **a**, Pathological scoring of apoptosis in intestinal tissues 3 weeks after BMT. Data from two experiments combined; $n = 10$ (TCD bone marrow only mice), $n = 9$ (BM + T (PBS)), $n = 8$ (BM + T (IL-22)); Kruskal–Wallis analysis. **b**, Representative haematoxylin and eosin staining of small and large intestines. Arrows indicate apoptotic cells within the intestinal epithelium. **c**, Splenocytes from recipients were analysed by flow cytometry 3 weeks after BMT, indicating frequencies of T cell subsets, expression of activation marker CD25, and expression of gut homing molecule $\alpha_4\beta_7$ integrin; $n = 9$ (PBS-treated) and $n = 10$ (IL-22-treated) mice per group; *t*-test analysis. **d**, Expression of inflammatory cytokines in spleen ($n = 9$ PBS-treated and $n = 10$ IL-22-treated mice per group) and SI ($n = 10$ mice per group) was analysed in recipient tissues 3 weeks after BMT; *t*-test analyses, multiple comparisons corrected for with Holm–Sidak correction. **e**, REG3β immunohistochemistry staining in SI samples of recipient mice 3 weeks after BMT, data representative of three experiments. **f–k**, RT–qPCR of relative mRNA expression in SI tissue samples of PBS-treated versus IL-22-treated mice 3 weeks post-BMT for: *Wnt3* (**f**); *Egf* (**g**); *Hes1* (from purified crypts) (**h**); *Rspo3* (**i**); *Ctnnb1* (from purified crypts) (**j**); *Axin2* (from purified crypts) (**k**); $n = 10$ mice per group for purified crypt samples; $n = 8$ (PBS-treated) and $n = 9$ (IL-22-treated) mice per group for whole SI tissue samples; Mann–Whitney *U* test. Data are mean and s.e.m.; $^*P < 0.05$, $^{**}P < 0.01$. Data combined from two independent experiments unless stated otherwise.

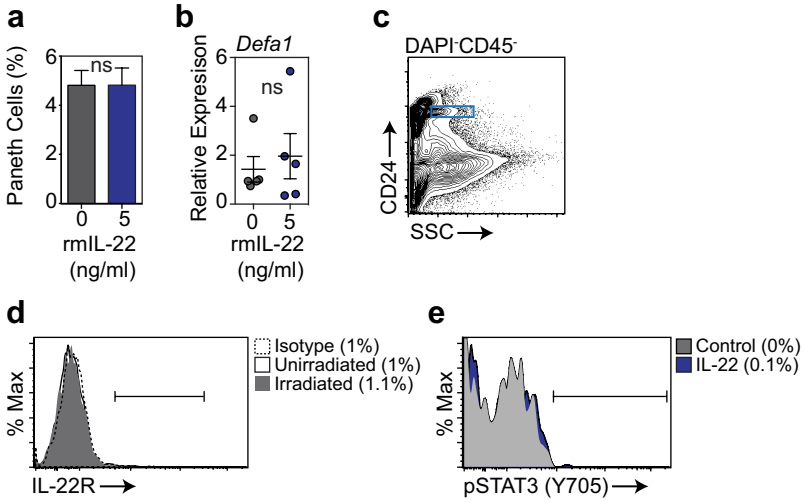

Extended Data Figure 7 | IL-22 does not enhance Paneth cell frequency, *Defa1* gene expression, or STAT3 phosphorylation *in vitro*. **a**, Percentage of Paneth cells in organoids cultured with/without 5 ng ml^{-1} rmIL-22 for 7 days, as evaluated by flow cytometry after dissociation into single cells; $n = 7$ independent cultures per group (one mouse per culture); *t*-test. **b**, RT–qPCR analysis of the relative mRNA expression of Paneth cell gene *Defa1* in SI organoids cultured with/without 5 ng ml^{-1} rmIL-22 for 7 days; $n = 5$ independent cultures per group (1–2 pooled mice per culture); Mann–Whitney *U* test. **c**–**e**, Paneth cell IL-22R expression and STAT3 phosphorylation assessed by flow cytometry. Shown are gating of Paneth cells based on side scatter and CD24 expression (**c**), Paneth cell IL-22R expression at baseline and 5 days after 1,200 cGy total body irradiation (one of two experiments) (**d**), and STAT3 phosphorylation in Paneth cells as determined by phosflow of dissociated crypt cells after a 20-min pulse with rmIL-22 (20 ng ml^{-1}, 37 °C; one of two experiments) (**e**). Data are mean and s.e.m. Data combined from at least four independent experiments unless otherwise stated.

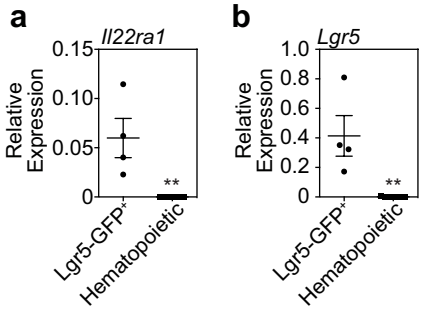

Extended Data Figure 8 | ISCs express *Il22ra1*. **a**, Relative mRNA expression of *Il22ra1* in sorted Lgr5–GFP$^+$ cells ($n = 4$ biological replicates), with various sorted haematopoietic populations serving as negative controls, including intestinal dendritic cells ($n = 4$), intestinal ILC3s ($n = 2$), and splenic B cells ($n = 1$). **b**, *Lgr5* mRNA relative to *Gapdh* expression in sorted Lgr5–GFP$^+$ cells and haematopoietic samples described above to confirm Lgr5 expression in sorted Lgr5–GFP$^+$ cells. Data are mean and s.e.m.; Mann–Whitney *U* test; $^{**}P < 0.01$.

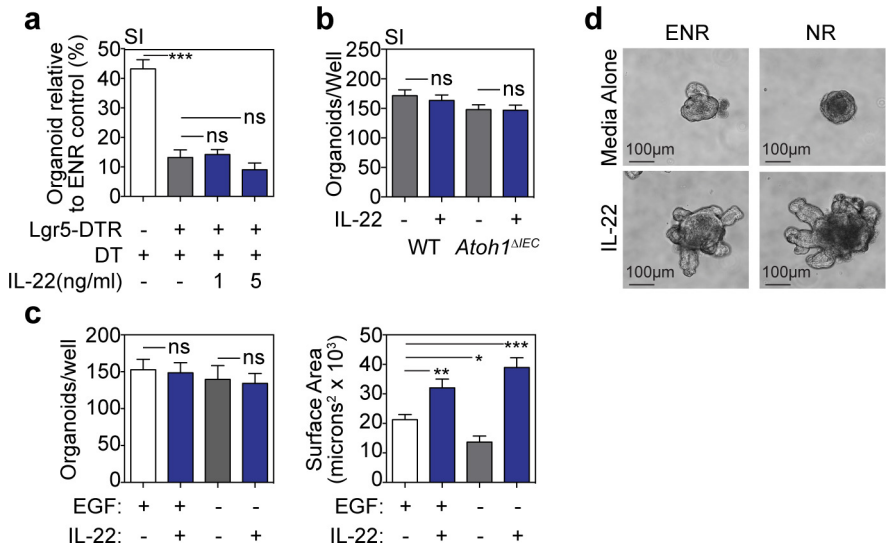

Extended Data Figure 9 | IL-22 increases the size of SI organoids cultured without EGF. a, Efficiency of wild-type and Lgr5-DTR SI organoid formation after culture with diphtheria toxin (1 ng μl^{-1}) to deplete Lgr5^{+} cells; one of three experiments; $n = 6$ (wild type), $n = 5$ (Lgr5-DTR), $n = 6$ (1 ng ml^{-1} IL-22), $n = 6$ (5 ng ml^{-1} IL-22) wells per group. **b**, Numbers of wild-type and *Atoh1*$^{\Delta IEC}$ day-7 SI organoids cultured with/without rmIL-22 (5 ng ml^{-1}); $n = 6$ wells per group. **c**, **d**, Omission of EGF from the standard ENR medium (NR). **c**, The effect of IL-22 on organoid numbers and size in the absence of EGF; $n = 6$ wells per group for numbers; $n = 45$ (ENR), $n = 37$ (ENR plus IL-22), $n = 42$ (NR), $n = 54$ (NR plus IL-22) organoids per group for size; data combined from three experiments. **d**, Brightfield images of wild-type SI organoid cultures in the presence or absence of EGF (50 ng ml^{-1}), representative of three experiments. Data are mean and s.e.m. Comparisons were performed with *t*-tests (two groups) or ANOVA (multiple groups); $^{*}P < 0.05$, $^{**}P < 0.01$, $^{***}P < 0.001$. Data combined from three independent experiments unless otherwise stated.

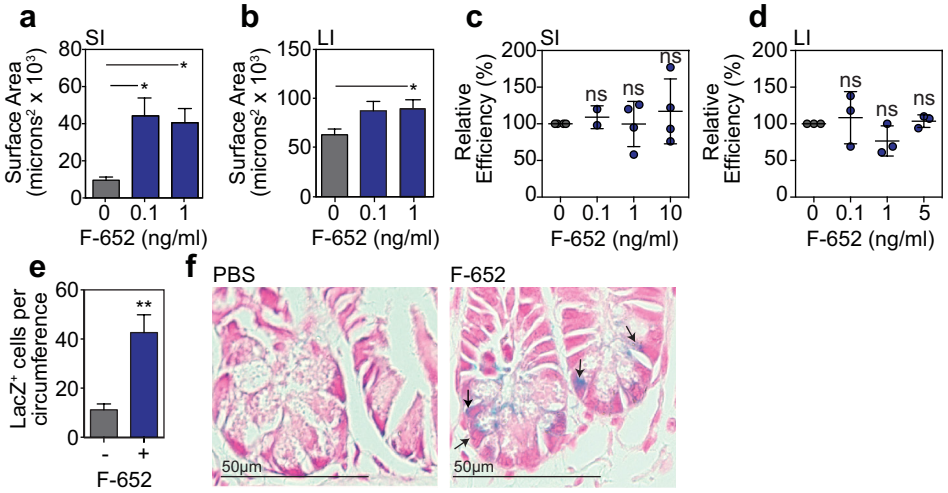

Extended Data Figure 10 | F-652 increases organoid size *ex vivo* and reduces radiation injury to the ISC compartment *in vivo*. **a**, **b**, Area of small (**a**) and large (**b**) intestine wild-type B6 organoids cultured with/without the rhIL-22-dimer and Fc-fusion molecule F-652; SI: $n = 37$ (0 ng ml^{-1}), $n = 60$ (0.1 ng ml^{-1}), and $n = 41$ (1 ng ml^{-1}) organoids per group combined from three experiments; LI: $n = 137$ (0 ng ml^{-1}), $n = 83$ (0.1 ng ml^{-1}) and $n = 132$ (1 ng ml^{-1}) organoids per group combined from two experiments; ANOVA. **c**, **d**, Organoid efficiency relative to control in cultures of B6 SI organoids ($n = 4$ wells per group combined from two experiments) (**c**) and B6 LI organoids ($n = 3$ wells per group; one of two experiments) (**d**) treated with different concentrations of recombinant human F-652; ANOVA. **e**, **f**, B6 Lgr5-LacZ mice were treated with PBS or F-652 (100 µg kg^{-1}), administered subcutaneously on the day of total body irradiation (10–12 Gy) and again 2 days later; one of three experiments. **e**, Lgr5-LacZ^{+} crypt cells per SI circumference were evaluated at day 3.5 after irradiation (10 Gy); statistics based on $n = 11$ independent sections (PBS-treated) versus $n = 14$ independent sections (F-652-treated) from irradiated mice; independent sections were derived from three mice per group; first dose of PBS or F-652 was administered 4 h before irradiation; Mann–Whitney *U* test. **f**, Representative crypt base images 3.5 days after irradiation (10 Gy). Arrows indicate Lgr5-LacZ^{+} crypt cells. Data are mean and s.e.m.; $^{*}P < 0.05$, $^{**}P < 0.01$.